HELSINKI UNIVERSITY OF TECHNOLOGY
Department of Mechanical Engineering

Mikko Keinänen

LATENT HEAT RECOVERY FROM SUPERCOOLED SODIUM ACETATE TRIHYDRATE USING A BRUSH HEAT EXCHANGER

Master's thesis submitted for evaluation as graduation work for the degree of Master of Science in Technology

Supervisor: Professor Markku Lampinen

Instructor: Ari Seppälä D.Sc.

Espoo, August 30, 2007

HELSINKI UNIVERSITY OF TECHNOLOGY

Abstract of the Master's Thesis

Author: Mikko Keinänen

Title of the Thesis:
LATENT HEAT RECOVERY FROM SUPERCOOLED SODIUM ACETATE TRIHYDRATE USING A BRUSH HEAT EXCHANGER

Date: August 30, 2007 **Number of Pages:** 104

Department: Department of Mechanical Engineering

Professorship: Ene-39 Thermal Engineering

Supervisor: Professor Markku Lampinen

Instructor: Ari Seppälä *D.Sc*.

This study is a part of a research project developing heat storages for warming automobile combustion engines. Thermal storage is charged with engine waste heat, which is discharged in order to maintain proper engine temperature or used for preheating.

The supercooling phenomenon intrigued us because of its ability to store the latent heat of phase change material (PCM) without any losses for long periods of time and release it when desired.

In this work, heat recovery as supercooled liquid sodium acetate trihydrate (SAT) encounters rapid phase change in the various brush heat exchangers is studied. Laboratory experiments uncover the suitability of supercooled sodium acetate trihydrate as a latent heat storage medium by output capacities and repeatability of the freeze–thaw cycles. An effect that the degree of supercooling and coolant flow rate has on the heat recovery is also considered.

Curved pipe heat transfer characteristics and optimal curvature for efficient heat transfer with adequate pressure losses was studied by minimizing the entropy generation rate in a heat transfer pipe.

Results revealed an exiguous relation between brush density and output capacities and heat recovery rate. For low power requirements, coarser brushes should be utilized, as the heat release rate is moderate. Crystallization experiments conducted in glass vessels compared to the ones performed in the brush heat exchangers showed a significant difference of the stability of the supercooled metastable state and the degree of supercooling. Thus, major work has to be pursued in developing stable and reliable supercooled phase change material, as spontaneous crystallization must be prevented.

Keywords: heat recovery, latent heat storage, supercooling, brush heat exchanger, sodium acetate trihydrate, curved pipe heat transfer

TEKNILLINEN KORKEAKOULU

Diplomityön tiivistelmä

Tekijä: Mikko Keinänen

Työn nimi:
LÄMMÖNTALTEENOTTO ALIJÄÄHTYNEESTÄ NATRIUMASETAATTI TRIHYDRAATISTA HARJALÄMMÖNVAIHTIMESSA

Päivämäärä: 30.8.2007 **Sivumäärä:** 104

Osasto: Konetekniikan osasto
Professuuri: Ene-39 Lämpötekniikka ja koneoppi

Työn valvoja: Professori Markku Lampinen

Työn ohjaaja: Ari Seppälä, TkT

Työ on osa tutkimusta, jossa kehitetään mm. lämmönvarastointiyksikköä ajoneuvojen moottorin ajonaikaisen lämpötilan ylläpitämiseksi sekä esilämmitykseen. Lämpövarasto ladataan moottorin hukkalämmöllä.

Aineen alijäähtymisilmiötä voidaan kätevästi hyödyntää moottorin esilämmittämisessä, jossa faasimuutosmateriaalin latenttilämpö voidaan varastoida häviöttömästi pitkiäkin aikoja ja vapauttaa haluttuna ajankohtana.

Työssä tutkitaan lämmöntalteenottoa, kun alijäähtynyt nestemäinen natriumasetaatti trihydraatti kokee nopean faasimuutoksen erilaisissa harjalämmönvaihtimissa. Laboratoriossa suoritetut kokeet paljastavat alijäähtyneen natriumasetaatti trihydraatin soveltuvuuden lämmönvarastointimateriaaliksi saatujen tehojen, lämpömäärien ja ilmiön toistettavuuden avulla. Lisäksi alijäähtymisasteen sekä jäähdytysveden virtausnopeuden vaikutuksia lämmöntalteenottoon tutkitaan.

Lämmönsiirto-ominaisuuksia kierteisissä putkissa ja optimaalista kierteisyyttä tehokkaan lämmönsiirron ja pienten painehäviöiden aikaansaamiseksi tutkittiin minimoimalla lämmönsiirrosta ja painehäviöistä johtuva entropian generoituminen.

Harjatiheyden vaikutus lämmöntalteenottoon jäi verrattain pieneksi. Harvemmat harjat ottavat lämpöä talteen pidemmän aikaa matalammalla teholla ja tiheämmät harjat lyhyemmän aikaa suuremmalla teholla. Lasi-astioissa suoritetut kiteytymiskokeet paljastivat suuren eron alijäähtymisen pysyvyyden ja alijäähtymisasteen osalta verrattuna harjalämmönvaihtimissa tapahtuneisiin kokeisiin. Sen johdosta, luotettavan ja stabiilin alijäähtyvän faasimuutosaineen kehittäminen on ensiarvoisen tärkeää, jotta spontaanisti tapahtuva kiteytyminen kyetään estämään.

Avainsanat: lämmöntalteenotto, faasimuutosvarasto, alijäähtyminen, harjalämmönvaihdin, natriumasetaatti trihydraatti, lämmönsiirto kierreputkessa

TABLE OF CONTENTS

NOMENCLATURE

a	Specific dimension (mm) (Fig. 5)
b	Specific dimension (mm) (Fig. 5)
c_p	Specific heat capacity (J/kgK)
C_r	Curvature ratio (Eq. 15)
D	Diameter of coil (m)
d	Diameter of heat transfer pipe (m)
De	Dean number
f	Friction factor coefficient
h	Enthalpy (J/kg)
He	Helical number
L	Total length of heat transfer pipe (m)
l	Latent heat of fusion (J/kg)
m	Mass (kg)
$\dot{m}_w$	Mass flow rate of water (kg/s)
Nu	Nusselt number
P	Circumference of heat transfer pipe (m)
p	Pressure (Pa)
Pr	Prandtl number
Q	Recovered heat (J)
r	Radius of heat transfer pipe (m)
Re	Reynolds number
$\dot{S}'$	Entropy generation rate per unit length (J/mK)
T	Temperature (K)
t	Time (s)
v	Velocity (m/s)
x	Mass fraction

α	Heat transfer coefficient (W/m²K)
β	Torsion parameter
δ	Curvature ratio (d_i/D)
ε	Efficiency
λ	Thermal conductivity (W/mK)
μ	Dynamic viscosity (kg/ms)
ρ	Density (kg/m³)
τ	Time (s)
φ	Heat transfer rate (W)
φ'	Heat transfer rate per unit length (W/m)

Subscripts

c	Crystallization
crit	Critical
cum	Cumulative
e	End
f	Friction
gen	Generated
h	Helical
i	In or Inner
L	Laminar
m	Melting
o	Out or Outer
p	Pressure or peak
q	Heat transfer
s	Straight or surface
sc	Supercooled

st	Steady state
T	Turbulent or temperature
t	Toroidal
w	Water

ABBREVIATIONS

BHX	Brush heat exchanger
CMC	Carboxymethyl cellulose
HT	Heat transfer
HTF	Heat transfer fluid
PCM	Phase change material
SA	Sodium acetate
SAT	Sodium acetate trihydrate

FOREWORD

In the course of this study I have learned an enormous amount about a variety of new and interesting areas. The unfamiliarity of the topic and the versatility of the research made it incredibly captivating and challenging. I hope the results gained through the novel nature of this research will impart preliminary knowledge that will be found useful in designing supercooled latent heat storages.

My honest compliments go to Ari Seppälä, with whom I pieced together a jigsaw puzzle piece by piece, and to laboratory technician Mika Ahlgren, whose skills and knowledge in engineering made this thesis possible. In addition, compliments go to Kari Saari and all the Applied Thermodynamic Laboratory personnel, and to Pertti Kauranen and the VTT work group for granting me this fascinating opportunity. I want to express my gratitude to Oy Hydrocell Ltd. for the brush heat exchangers. This project was financed by Finnish Funding Agency for Technology and Innovation (Tekes), the Technical Research Center of Finland (VTT), Lumikko Oy, VAK Oy, Eurocon Oy, Red Cross Finland Blood Service, Finland Post Corporation, Easy Km Oy and EHS Group Oy and it is part of the Tekes' ClimBus technology program for mitigating climate changes.

I also want to thank my parents for appeasing my basic needs and my friends for taking my mind off my work in moments of desperation.

To my father

Espoo, August 2007

Mikko Keinänen

1 INTRODUCTION

With growing energy consumption and higher energy prices, new energy saving methods are needed. One approach to improving energy efficiency is the exploitation of waste heat. Energy storage plays an important role in the utilization of such a system. Thermal energy storage especially has become one major topic of research over the last twenty years. Short-term storage of only a few hours or long-term storage of a few months is essential in some applications. Thermal energy storages can store energy to be utilized in times when no other method is available or to meet peak energy demands.

Heat absorbed and released as the result of phase change has been used for centuries; accordingly, modern power plants utilize the phase change of water. Phase change materials (PCMs) are prime candidates for use as thermal energy storage media because of their superior energy storage capacities. Compact heat storages with PCM have many advantages over traditional sensible heat storages. Many applications already exploit phase change materials, but more remain to be developed.

The Technical Research Center of Finland (VTT) launched a research project in July, 2006 to develop cold and heat energy accumulators for motor vehicles. The objective is to reduce exhaust gases emitted by engines and diesel-driven refrigerating machines in trucks, lower the noise problem related to these apparatuses and spare expenses. PCM was chosen as a method of storing the cold or heat energy in accumulators.

Heat storage mounted on vehicles depresses the negative factors related to the cold starting of internal combustion engines. These are increased fuel consumption, high concentration of CO and hydrocarbons in exhaust gases, decrease of engine operating time and high load on battery and starter. Latent heat thermal energy storage can store waste heat from the engine and release it at the next cold start.

Particularly for cold start applications, it would be an advantage to be able to discharge the heat as desired. The so-called “heat on demand” approach can be achieved with supercooled storage material. The discharge of supercooled PCM could be triggered externally to warm the engine before ignition. Related experimental and numerical research by Vasiliev et al. (2000) into preheating automotive engines with latent heat storage modules without supercooling phenomena suggested promising results. The bus petrol engine was warmed from –10 ºC to 20 ºC in less than 7 minutes with 65 kg of sodium hydroxide hydrate ($NaOH \cdot H_2O$).

Latent heat thermal storages have the advantage of high energy density and near isothermal discharge temperature. However, a major weakness is the poor heat conduction of PCM, which limits the heat transfer rate. Finned heat exchangers have been proposed to enhance the heat transfer. A special and challenging characteristic of supercooled thermal storages is the unpredictable behavior of supercooled liquids.

This study investigates experimentally the suitability of sodium acetate trihydrate (SAT) in brush heat exchangers (BHX) for heat recovery. The target is to examine the heat transfer rate, quantity of recovered heat, and thermal stability of heavily supercooled sodium acetate trihydrate using various brush heat exchangers. The effect of the supercooling level on heat recovery with several heat transfer fluid (HTF) velocities is presented. Transparent containers allowed visual examination of the phase change phenomenon and few surprises were encountered. In addition, heat transfer characteristics of slightly curved pipes are concisely discussed. A video showing supercooled crystallization of sodium acetate trihydrate in a brush heat exchanger can be found on the laboratory’s web page: (ref. August 2007) http://www.termo.hut.fi/research/faasimuutos/kiteytyminen.html
In the video, temperature of supercooled SAT rises from 30 ºC to the melting temperature of 58 ºC in few minutes.

2 LATENT HEAT THERMAL STORAGES

High energy density and isothermal discharge temperature makes latent heat storages superior to sensible heat storages. For example, water has to cool 80 degrees to release the same quantity of energy than when it freezes. At a macroscopic level, phase changes may be categorized by discernible phases:

- Solid ↔ Liquid
- Liquid ↔ Gas
- Solid ↔ Gas
- Solid ↔ Solid (alterations in crystal structure)

A significant method for practical phase change storages is solid–liquid phase change because of the simplicity of technical solutions, although energy stored on vaporization is an order of magnitude greater. Solid–solid phase changes are theoretically interesting, but the related enthalpy differences are typically diminutive (Peippo, 1989).

The daily and seasonal variations in available solar radiation impair the solar heating applications and, for that reason, thermal energy storages are mandatory for functional exploitation. An important study to develop low temperature latent heat thermal storages is in progress; this may help the final breakthrough in solar heating.

The temperature range of latent heat thermal storages varies with the melting or vaporizing temperatures of different phase change materials. Practical temperatures reaching from –30 ºC to 900 ºC ensures the wide range of applications for PCM storages.

2.1 Phase change materials

Common demands on phase change materials are large amounts of latent heat and high thermal conductivity. They should also have an eligible melting temperature in a practical

range, melt congruently with usually minimal supercooling and be chemically stable, low in cost, non-toxic and non-corrosive. Materials proposed as phase change materials after forty years of study are hydrated salts, paraffin waxes, fatty acids and eutectics of organic and non-organic compounds.

The most auspicious PCMs are salt hydrates and paraffin waxes. Commercial paraffin waxes are cheap with moderate thermal storage densities and have a wide range of melting temperatures. They melt without phase segregation, are chemically stable and undergo negligible supercooling. The low thermal conductivity (~0,2 W/mK) however limits their applications.

Hydrated salts are attractive materials due to their large amount of latent heat, relatively high thermal conductivity (~0,5 W/mK) and low cost. Phase segregation, supercooling, corrosivity, lower density compared to paraffin waxes and unstability on cycling are major problems related to salt hydrates. The large amount of latent heat, high thermal conductivity and supercooling abilities made the use of salt hydrate in these experiments attractive.

2.1.1 Sodium Acetate Trihydrate

Sodium acetate trihydrate (SAT) –$CH_3COONa \cdot 3H_2O$– was selected as the heat storage medium for this study, because of its considerable supercooling ability and high latent heat of fusion. Sodium acetate trihydrate is used on commercial heat pads where supercooled liquid is crystallized by clicking a metal disc inside the pad. Instantly, the temperature of the pad rises to around 58 ºC.

The only stable[1] hydrate – the SAT– of sodium acetate contains 60,28 wt% sodium acetate (SA) and 39,72 wt% water. The trouble with the SAT and other salt hydrates are their tendency of incongruent melting, corrosivity and the number of cycles they can withstand without any degradation in their thermal properties.

[1] The salt contain a specific number of water molecules loosly attached

Figure 1 presents the binary phase diagram of sodium acetate and water. When heating SAT (blue line) from point *a* toward point *b*, at point *b peritectic reaction*[2] occurs, melting the salt incongruently. This generates anhydrous sodium acetate and liquid sodium acetate trihydrate. With continued heating, the anhydrous salt melts completely at point *c*. The composition of solution trails the line from *p* to *c*. Mass fractions of dehydrated salt and solution can be obtained from the lever rule. Point *p* is called the *peritectic point*.

The formed heavier anhydrous salt precipitates on the bottom of the container by gravity. On crystallization, the rehydration starts at the solution-precipitate interface. The formed hydrated crystals form a contact barrier between the anhydrous salt and the liquid solution and thus the crystallization cannot proceed further (Gök et al.). If point *b* would cross the melting line at point *p*, the salt would melt congruently. Therefore by adding more than 3,8 wt% of extra water to SAT, the formation of anhydrous salt can be prevented (see Fig. 1). However, thermal storage properties of the solution deteriorate with increased water content, as can be seen in Table 1.

Table 1. Thermal and physical properties of sodium acetate trihydrate and water mixtures (Lane, 1984; Tamme, 1984; Araki et al., 1995; Seppälä, 2007a).

Composition (wt- %)		Melting temperature (°C)	Latent heat (kJ/kg)	Specific heat (kJ/kgK), 58 °C		Density (kg/m³), 58 °C		Thermal conductivity (W/mK), 58 °C	
SAT	H_2O			Solid	Liquid	Solid	Liquid	Solid	Liquid
100	-	57–58,5	260 ± 11	2.79	3.0	1450	1280	0.7	0.4
95	5	56,5	220 ± 9	-	-	-	-	-	0.41
90	10	54.5–56	190 ±10	2.85	3.1	-	-	0.6	0.43
80	20	49–50	100	-	-	-	-	-	0.44

[2] Upon heating, one solid phase transforms into a liquid phase and another solid phase (Callister, 2003)

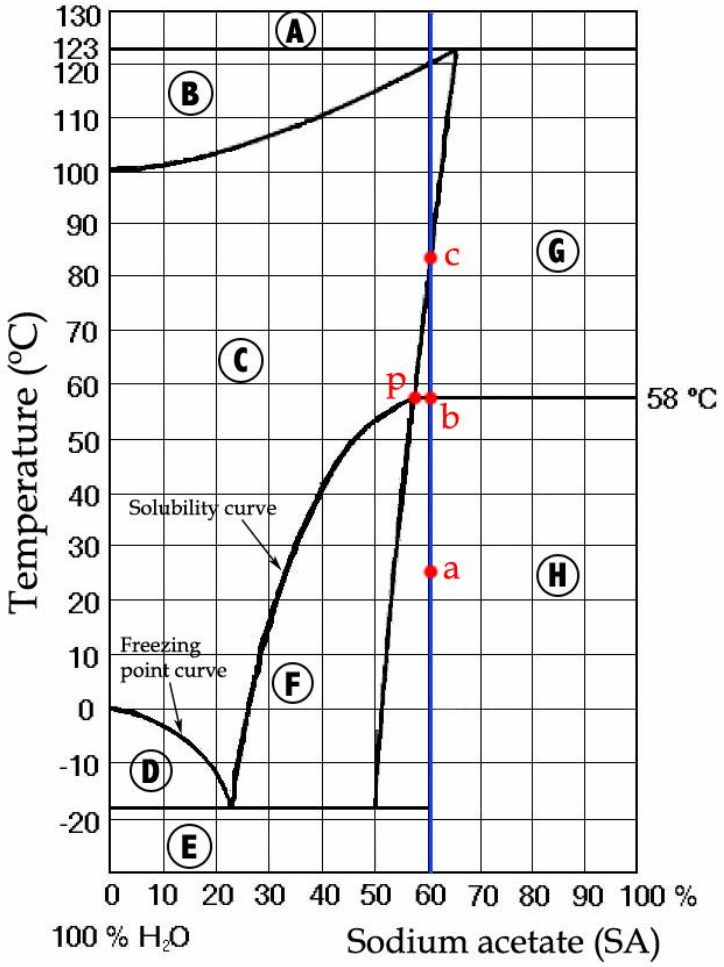

Figure 1. Phase diagram of sodium acetate and water. **A:** Vapor, **B:** Anhydrous sodium acetate and water vapor, **C:** Liquid sodium acetate solution, **D:** Sodium acetate in liquid state and water in solid state, **E:** Water in solid state and sodium acetate trihydrate, **F:** Solid sodium acetate trihydrate with excess liquid water (not supercooled), **F:** Liquid sodium acetate trihydrate and water (when supercooled), **G:** Anhydrous sodium acetate in liquid, brine type of phase, **H:** Solid sodium acetate trihydrate and solid anhydrous sodium acetate (not supercooled), **H**: Liquid sodium acetate trihydrate with precipitate of anhydrous sodium acetate (when supercooled). Picture modified from Watson, 1973.

A more effective method of avoiding phase segregation is to add gelling or thickening material into the solution to hinder the heavier anhydrous salt in sinking to the bottom of the container. Also, mechanical stirring and capsulation of the PCM averts the phases separating.

Wada et al. (1984) investigated the thermal stability of SAT after several freeze-thaw processes with different compositions. Sample A comprised guaranteed grade SAT, sample B comprised technical grade SAT and sample C technical grade SAT thickened by using polyvinyl alcohol. All three samples also comprised nucleating agents to prevent supercooling. Results illustrated that the latent heat storage capacity of samples A and B, without thickening agent, substantially decreased after 400 cycles of sample A from 250 kJ/kg to 160 kJ/kg and of sample B from 250 kJ/kg to 200 kJ/kg, whereas sample C, with thickening agent, showed no decrease at all during thermal cycling. What is more, the technical grade SAT (sample B) performed better than guaranteed grade SAT (sample A). Wada et al. suggested that this is due to the fact that the impurities in technical grade SAT prevents anhydrous sodium acetate particles from growing.

2.2 Thickening agent carboxymethyl cellulose

To prevent phase segregation, carboxymethyl cellulose (CMC) $–C_6H_9OCH_2COONa–$ (VWR Prolabo) was added in this study to the compound of water and SAT (Choi et al., 1996). Thickening increases the viscosity and thereby holds the solution together. Consequently, the anhydrous salt, generated while melting, has a greater chance of contacting water so that the rehydration of the salt can occur when crystallized (Gök et al.). In addition, up to around 3 wt %, the thickening agent increases the latent heat of SAT water solution (Tamme, 1984). The increase in latent heat may be explained by the higher amount of salt hydrate participating in the phase change process.

Cabeza et al. (2003) used various thickening agents with SAT and reported that cellulose made more suitable material than SAT thickened with starch or bentonite. However, with methylhydroxyethyl cellulose (MHE-cellulose) and methyl cellulose (M-cellulose), after a few cycles the salt hydrate and the cellulose separated. The problem was solved using a maximum heating temperature of 65 ºC. They also reported a 20 % to 35 % decrease in latent heat, but the amount of cellulose was large (15 wt% or 30 wt %).

3 SUPERCOOLING AND CRYSTALLIZATION

As solutions with an initial temperature above their melting point cool down and reach the crystallization (freezing) temperature, thermodynamics favors the solidifying. However, often solutions remain liquid, supercool, and attain metastable state. For example, in the laboratory, extremely pure liquid water has been able to cool down to –41 ºC at atmospheric pressure (Angell, 1982).

Supercooling is not a very well known topic, even though it is common in nature, where supercooled water appears in clouds, trees, minerals, insects and fishes. Some insects survive the cold season by preventing the supercooled water in their system from crystallizing. Small fishes living in cold salty waters (–2 ºC) can live only by controlling the permanently supercooled blood in their circulation. Clouds in colder climates are formed when ascending humid air cools and become saturated and water vapor condenses when in contact with condensation nuclei. Higher clouds ranging from 5–13 km have a scarcity of nucleating agents and therefore water can supercool well below 0 ºC. Accordingly, supercooling of water plays a major role in the phenomena that determine the climate on Earth (Debenedetti, 1996).

In technology, supercooled water has been used to store isolated proteins for use in therapeutic or biochemical applications. Supercooled phase change storages have been proposed for the use of solar thermal energy applications (Watson, 1973). Commercial heat pads provide low temperature heat for people settling in colder climates as well as for health–related purposes. Accordingly, at some level, supercooling can be controlled, but the technical applications are still few in number.

Metastable liquids, whether supercooled, superheated or supersaturated, are in a state of precarious equilibrium where a minor external disturbance may trigger the formation of a new phase and drive the system toward a condition of greater stability. Although respectable theories of metastable liquids exist, the calculation of thermophysical properties still remains an open problem (Debenedetti, 1996).

Altogether, for supercooled heat storages, it is important that the supercooled PCM is capable of reliable nucleation when it is required to liberate the latent heat of crystallization; but it is also important that the PCM has a large amount of activation energy for nucleation to avoid a spontaneous crystallization of supercooled condition (Arrhenius et al., 1982).

3.1 Heterogeneous and homogeneous nucleation

Nucleation is the onset of phase transition in a small area. In most practical circumstances, solid surfaces, suspended particles or microscopic bubbles act as nucleation sites for heterogeneous nucleation of liquid or vapor to commence. This process, heterogeneous nucleation, limits the level of supercooling in the real world. The avoidance of heterogeneous nucleation is one major criterion for exploitation of supercooled thermal storages.

A much less common manner of phase transition is homogenous nucleation. In homogenous nucleation, superheated or supercooled fluid, in the absence of impurities or solid surfaces, experiences spontaneous density or composition fluctuations forming embryos of a new phase. As embryos attain the critical size, the new phase is formed spontaneously. Homogenous nucleation determines the practical, attainable limits of liquid superheating or supercooling (Debenedetti, 1996; Mullin, 2001).

3.1.1 Thawing and crystallization of sodium acetate trihydrate

The phase change mechanisms of salt hydrates on heating can be observed in two steps. In the first step, as solid SAT is heated to around 50 ºC, water of crystallization begins to release from the lattice of the salt hydrate. In the second step, anhydrous salt dissolves in its released water of crystallization. In the case of SAT, these steps occur simultaneously. The first step is endothermic, in nature whereas the second is exothermic. The latent heat of phase change is the remainder of the endothermic and exothermic processes taking place (Sharma et al., 1990).

If the anhydrous component completely dissolves in its water of crystallization, the salt is called *congruently melting* salt and, in the case of the partly dissolving anhydrous component, the melting is called *incongruently melting* salt. SAT is categorized as *incongruently melting* or, in some references, as *semicongruently melting* salt (Sharma et al., 1990).

From thermodynamics it can be calculated what fraction of supercooled sodium acetate will crystallize depending on the degree of supercooling. In the adiabatic process ($\Delta H = 0$), the enthalpy of supercooled liquid can be calculated with the Equation (1), which can be expressed also with Equation (2).

$$h_{l,T_{sc}} = x h_{s,T_m} + (1-x) h_{l,T_m} \tag{1}$$

$$x = \frac{h_{l,T_m} - h_{l,T_{sc}}}{h_{l,T_m} - h_{s,T_m}} = \frac{\int_{T_{sc}}^{T} c_{p,l}\, dT}{l(T_m)} \tag{2}$$

where x is the fraction of formed solid, h_{s,T_m} and h_{l,T_m} the enthalpies of solid and liquid PCM at melting temperature, $h_{l,T_{sc}}$ the enthalpy of liquid PCM at supercooled temperature, $c_{p,l}$ the heat capacity of liquid PCM and $l(T_m)$ the latent heat at the melting temperature. Equation (2) can be approximated by the following equation if heat capacity is nearly constant in the temperature range

$$x \approx \frac{c_{p,l} \Delta T_s}{l_{SAT}} \tag{3}$$

where ΔT_s is the degree of supercooling. According to Equation (3), pure SAT, with latent heat of 260 kJ/kg and specific heat capacity of 3 kJ/kg, could be supercooled to a temperature of –28,7 ºC (ΔT_s = 86,7 ºC; T_m = 58 ºC) and yet all liquid SAT would crystallize to solid.

4 BRUSH HEAT EXCHANGERS

Brush Heat Exchangers (BHX) are a novel type of heat exchangers developed in cooperation with Helsinki University of Technology Applied Thermodynamics Laboratory and Oy Hydrocell Ltd. Originally they were designed for hydrogen accumulators, but their range of applications has been extended to include indoor air-conditioning. The advantages of BHXs are a large shell-side heat transfer area and the versatility to revise the shape of the heat exchanger as desired (Häggblom, 2002).

Latent heat thermal storages suffer from low thermal conductivities of the heat storage medium, preventing rapid heat transfer between heat transfer fluid and PCM. The structure and large heat transfer area of BHXs was thought to be ideal for enhancing the heat transfer of latent heat storage. Because of the corrosivity of SAT (Farrell et al., 2006 & Cabeza et al., 2002), heat transfer pipes were made from stainless steel and brushes from aluminum. The containers of the tube brush heat exchangers were made from transparent acrylic tube to allow a visual inspection of the heat storage medium. Table 2 illustrates the characteristics of the heat exchangers used. 'Tank BHX' refers to the first BHX with an aluminum container and 'Tube BHX A–C' to the heat exchangers with a transparent acrylic tube container; A has the coarsest brushes.

Table 2. Characteristics of the brush heat exchangers used.

Name of BHX	Mass of brushes (g)	Diameter of brush filament (mm)	Length of brush filament (mm)	Inlet and outlet diameter of HT pipe (mm)	Total length of HT pipe (m)	Number of HTF inlets	Heat transfer area m²	Diameter of PCM tube (mm)	PCM capacity (dm³)
Tank	210	0,27	150	7/9	0,56	1	1,15	140	2.8
Tube A	110	0,27	56	4/6	1,21	2	0,65	70	1.8
Tube B	177	0,27	56	4/6	1,35	2	1,05	70	1.8
Tube C	217	0,27	56	4/6	1,35	2	1,29	70	1.8

Figure 2. Cut tank brush heat exchanger.

Tank BHX (Fig. 2) only had one heat transfer pipe twisted on helix, making a loop at the bottom of the container. Since incoming hot and outgoing cold HTF pipes are in contact with each other, the effect on efficiency can only be imagined. The problem was recognized and the tube BHXs were made out of two heat transfer pipes with two inlets and outlets, as shown in Figure 3.

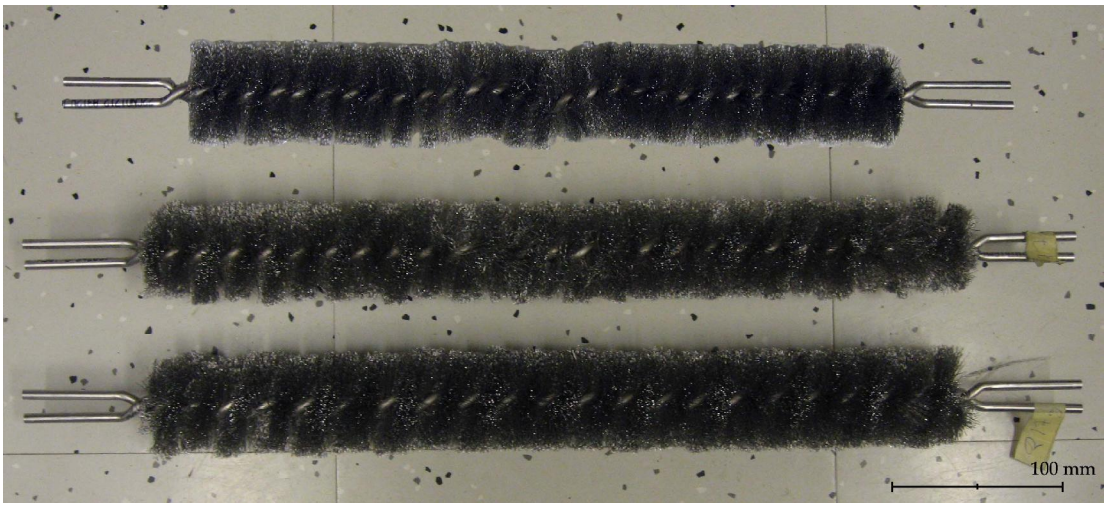

Figure 3. Brush heat exchangers A–C without the acrylic tube.

5 HEAT TRANSFER IN BRUSH HEAT EXCHANGER

As discussed earlier, a major disadvantage of latent heat storages is the low thermal conductivity of PCM, which significantly reduces the heat transfer rate. Crystallized material on heat transfer surfaces acts as a heat transfer insulator. In principle, there are two ways of solving this problem. One the one hand, the distances for heat transfer by conduction in the PCM can be shortened by encapsulating the material or by using highly dispersed heat exchangers with short distances between their fins or pipes. On the other, the thermal conductivity of the PCM can be enhanced by embedding highly conductive particles into the PCM (Heinz & Streicher). Several researchers have studied the heat transfer enhancement of thermal energy storages: Choi et al. (1996) used circular fins, Ettouney et al. (2004) metal screens and metal spheres, Fukai et al. and Hamada et al. (2003 & 2005) carbon fibers and chips and Stritih rectangular fins. Kamimoto et al. (1985) and Mettawee and Assassa (2007) dispersed salt with highly conductive particles.

“Heat transfer in latent heat storage is a transient, non-linear phenomenon with a moving solid–liquid interface generally referred as the ‘moving boundary’ problem” (Lamberg et al., 2004). Therefore analytical solutions exist only for a couple of simple geometries and simple boundary conditions. The most famous analytical solution for the one-dimensional moving boundary problem is called the *Stefan problem*. However, the analytical or numerical solutions of phase change heat transfer are beyond this thesis and heat transfer is only dealt in a simple way.

5.1 Heat transfer enhancement in phase change medium

The large heat transfer area of brush heat exchangers enhances the rate of heat transfer in phase change material. Thermal conductance of the heat storage media increases with the increase of the volume fraction of brushes. In proportion, the energy storage capacity accordingly decreases. The ratio of brush filament volume versus energy storage capacity should be optimized.

Natural convection is the dominant heat transfer method in the liquid PCM phase and in melting. Fukai et al. (2000) reported that carbon brushes suppress this phenomenon. However, the brushes increase conduction heat transfer to significantly increase the total heat transfer of the liquid phase and melting. According to Fukai et al. (2000), 2 volume percent of carbon fibers guaranteed corresponding melting time of paraffin wax than with pure wax without carbon fibers.

On crystallization brushes intensify the conduction heat transfer and decrease the time of crystallization as the volume fraction of the brushes increases. Contrary to the melting process, natural convection can be ignored in solidification (Stritih, 2004). Fukai et al. (2000) reported that the length of the carbon fibers has an insignificant effect on thermal responses.

5.2 Recovered latent heat

On crystallization of supercooled sodium acetate trihydrate abruptly raises the temperature of the PCM from the supercooled temperature, denoted as T_{sc}, to peak crystallization temperature, denoted as $T_{c,p.}$ This heat is transferred through the metal brushes and pipe to the heat transfer fluid. The heat transfer rate or output capacity of the heat exchangers can be calculated when inlet and outlet temperatures of the heat transfer fluid and mass flow rate are known.

$$\varphi = c_{p,w} \dot{m}_w \Delta T_w \qquad (4)$$

where $c_{p,w}$ is the specific heat capacity of water, $\dot{m}_w$ the mass flow rate of water and ΔT_w the temperature change of water. Because of the nature of the unsteady state heat transfer; power φ is calculated in every time step. The recovered heat is obtained by multiplying the average heat transfer rate of sequential measurements with the time interval for every time step

$$Q = \varphi \Delta t \qquad (5)$$

The temperature difference between cooling water and the onset temperature of the crystallization and or the final temperature of the PCM affect the amount of recovered heat as sensible heat is also considered. Mainly in the experiments, the onset temperature of the crystallization was higher than the cooling water temperature. Thus, if only the recovered latent heat is considered for better comparability, the sensible heat of supercooled liquid should be reduced from the recovered cumulative heat. Figure 4 presents a typical temperature curve as supercooled SAT crystallizes at a higher temperature than the cooling water flow. At moment τ_1, the PCM crystallizes from the supercooled temperature T_{sc} to the peak temperature of $T_{c,p}$. The blue line is the inlet water temperature. At moment τ_e, the temperature of the PCM is the same as the water flow ($T_e = T_{w,i}$) and measurement is stopped. Consequently, the cumulative recovered latent heat is defined by

$$Q_{cum} = \int_{\tau_1}^{\tau} \varphi(t)dt - c_{p,l} m\Delta T \qquad (6)$$

where τ is the time at a certain moment and τ_1 is the onset time of crystallization, $c_{p,l}$ the specific heat capacity of liquid PCM, ΔT the temperature difference of the onset temperature of crystallization and the temperature of the cooling water and m the mass of PCM. Accordingly, if the final temperature of the PCM is higher than the cooling water temperature, the specific heat of the solid PCM multiplied by the temperature difference should be added in Equation (6). When time τ in Equation (6) is the ending time τ_e, the calculated cumulative heat presents the latent heat of the PCM times the mass of the PCM.

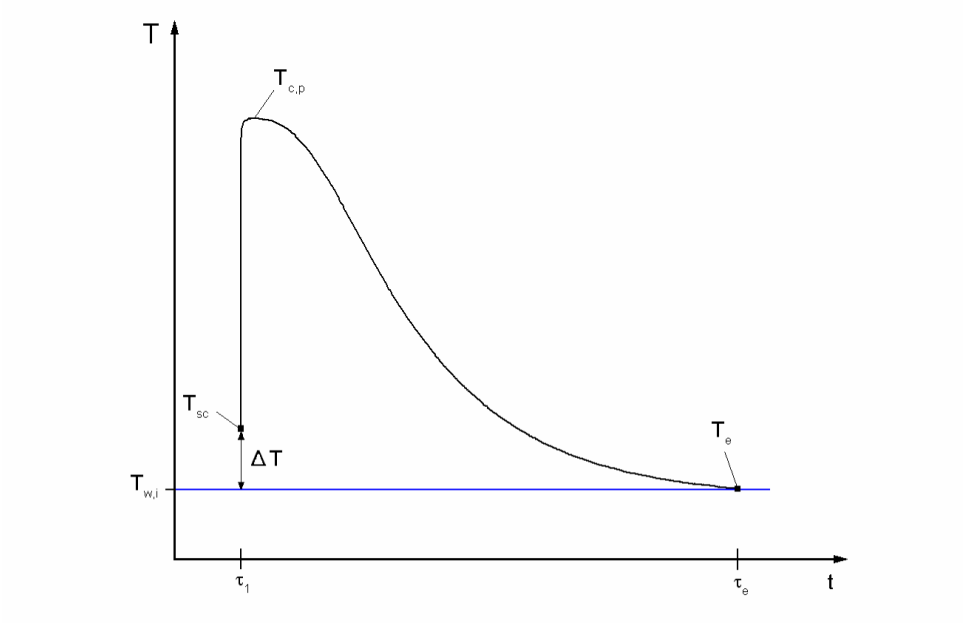

Figure 4. Temperature curve as supercooled PCM crystallizes (T_{sc} = supercooled temperature, $T_{c,p}$ = peak crystallization temperature, T_e = end temperature, $T_{w,i}$ = cooling water inlet temperature, τ_1 = time of crystallization, τ_e = experiment ending time).

The average heat transfer rate equalizes the apex of specific output capacity curves and presents better visualization. Besides, average heat transfer curves reveal the amount of power recovered in a certain time. The average output capacity during period of τ_1 to τ_j is given by

$$\overline{\varphi}(t = \tau_1 \rightarrow \tau_j) = \frac{Q_{cum}}{(\tau_j - \tau_1)} \qquad (7)$$

5.3 Flow characteristics in helical pipe

Several investigations have been conducted regarding fluid flow in a curved, helical or spiral pipes. A review by Naphon and Wongwises (2006) may be referred to. Flow in curved pipe is a complicated event and differs from that in a straight pipe as secondary flow is introduced by centrifugal forces. Visualization of the flow is provided by Yamamoto et al. (2002) both numerically and experimentally. Accordingly, the secondary flow enhances

heat transfer but increases pressure drop. These parameters are, though, greatly dependent on the curvature and torsion of the pipe. Curvature is the wavelike shape of the pipe in x-y –plane (Fig. 5) and torsion adds one dimension as it presents the twist around x-axis. Nevertheless, while the number of studies is great, research on pipes with large curvature and torsion, as in the case of BHXs, is limited.

For curved pipes, Dean (1927) non-dimensionalized the simplified Navier–Stokes equations for torus of small curvature ratio and arrived at dynamical similarity parameter $K = 2Re^2(d_i/D)$, where d_i is the inner diameter of the pipe and D the diameter of the torus. The square root of half of the K was later called the *Dean number* and is defined by

$$De = \mathrm{Re}\left(\frac{d_i}{D}\right)^{1/2} \tag{8}$$

where Re is the Reynolds number given by

$$\mathrm{Re} = \frac{\rho d v}{\mu} \tag{9}$$

where ρ is the density of the fluid, d the inner diameter of pipe, v the flow velocity and μ the dynamic viscosity of the fluid.

The Dean number characterizes the ratio of the centrifugal force to the viscous force. Germano (1989) showed that the Dean equations, when extended to helical pipe flow, contain not only the Dean number but torsion as well. Also, Chen and Jan (1992) verified this and suggested that the flow in a helical pipe is controlled by three parameters: Reynolds number, Dean number and torsion number $2\tau Re$, where non-dimensional torsion τ is defined by Equation (16). Figure 5 shows the schematic cutaway diagram of one heat transfer pipe, where the characteristic dimension a is the perpendicular distance of the 2D plane between the center line of the helical coil and helical pipe, b the pitch of the helical

coil, d_i is the inner diameter of the pipe and D the diameter of the coil. The relation (d_i/D) is known as curvature or the curvature ratio and is denoted with the symbol δ.

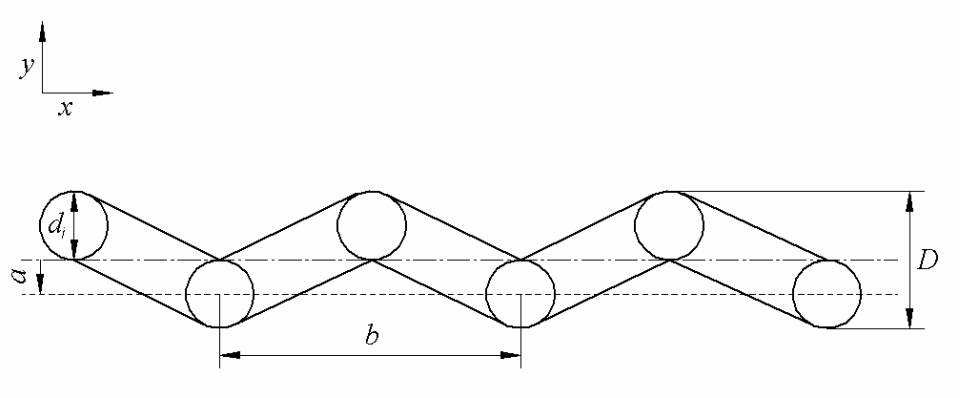

Figure 5. Schematic 2D diagram of curved heat transfer pipe.

5.3.1 Heat transfer coefficient

Several correlations of the Nusselt number for helical coils with small curvature (d_i/D) have been suggested, but for large curvature none was found. Abedin (2004) discussed and experimentally studied the heat transfer coefficient in analogous BHX's pipes with air as HTF. Abedin's equation for the Nusselt number in air flow was modified by Seppälä (Seppälä, 2007c) to gain a correlation for the water flow:

$$Nu = 0{,}00869 De^{1{,}076} \mathrm{Pr}^{0{,}175} \qquad (10)$$

where De is the Dean number by Equation (8) and Pr the Prandtl number. Kalb and Seader (1974) came with a numerical solution of the Nusselt number with constant wall temperature:

$$Nu = 0{,}836 De^{0{,}5} \mathrm{Pr}^{0{,}1} \qquad (11)$$

which is valid for $80<De<5000$, $0{,}007<d_i/D<0{,}1$ and $0{,}7<Pr<5$. Manlapaz and Churchill (1981) proposed Nu for fully developed flow with constant wall heat flux

$$Nu = \left[\left(\frac{48}{11} + \frac{51/11}{\left(1 + \frac{1342}{\mathrm{Pr}\, He^2}\right)^2} \right)^3 + 1{,}816 \left(\frac{He}{1 + \frac{1{,}15}{\mathrm{Pr}}} \right)^{3/2} \right]^{1/3} \qquad (12)$$

Where the helical number *He* is given by

$$He = \frac{De}{\left[1 + \left(\frac{b}{\pi D}\right)^2\right]^{1/2}} \qquad (13)$$

Dravid et al. (1971) numerically investigated the effect of secondary flow on laminar flow heat transfer (50<*De*<2000, 5<*Pr*<175), both in the fully developed region and in the thermal entrance region. A correlation, validated with experiments, was proposed

$$Nu = \left(0{,}65\sqrt{De} + 0{,}76\right)\mathrm{Pr}^{0{,}175} \qquad (14)$$

5.3.2 Friction factor and critical Reynolds number

Yamamoto et al. (1995) studied experimentally the effect of curvature and torsion of a helical pipe on the friction factor and critical Reynolds number. As distinct from other similar studies, they used a helical tube of large curvature and torsion (small *D*). They defined non-dimensional curvature C_r (Fig. 5) by

$$C_r = \frac{r_i a}{b^2 - a^2} \qquad (15)$$

The non-dimensional torsion τ and the torsion parameter β are defined by

$$\tau = \frac{r_i b}{b^2 + a^2} \tag{16}$$

$$\beta = \frac{\tau}{\sqrt{2C_r}} \tag{17}$$

For the three tube brush heat exchangers r_i = 2 mm, a = 3 mm and b = 27,6 mm, which corresponds to values of C_r = 0,008, τ = 0,07 and β = 0,57, respectively. The values are well within the range of the experimental study of Yamamato et al. (1995) and accordingly the friction factor for laminar and turbulent flow may be gained. For laminar flow (0 < *Re* < 2200), the friction factor agrees well with the theoretically obtained equation for a toroidal pipe (β = 0) by Yanase et al. (1989) and is given gy

$$f_{t,L} = f_{s,L}\left[0{,}0938\left(\mathrm{Re}\sqrt{\mathrm{C_r}}\right)^{1/2} + 0{,}557\right] \tag{18}$$

where $f_{s,L}$ is the friction factor of a straight tube, which can be calculated from the Hagen-Poiseuille equation.

$$f_{s,L} = \frac{64}{\mathrm{Re}} \tag{19}$$

For fully turbulent flow (Re > 8000), no theoretical equation is known (Yamamoto et al., 1995), but in the current case, the friction factor compared to the known toroidal friction factor is approximately 5 % larger. The friction factor for turbulent flow in a toroidal pipe is defined by

$$f_{t,T} = \frac{0{,}316\sqrt{C_r}}{\left(\mathrm{Re}\,C_r^2\right)^{0,2}} \tag{20}$$

For the helical pipe, in this study, Equation (20) is multiplied by a factor 1,05.

$$f_{h,T} = \frac{0{,}3318\sqrt{C_r}}{\left(\mathrm{Re}\, C_r^2\right)^{0{,}2}} \qquad (21)$$

Generally, Yamamoto et al., (1995) points out that with fixed curvature C_r, and increasing torsion parameter β (increasing pitch), the friction factor deviates from that of a toroidal pipe and decreases toward that of a straight pipe as torsion increases even further. The friction formula (20) (and 21) for a toroidally curved pipe may only be applicable to a helical pipe whose torsion parameter β is smaller than 0,5.

Yamamoto et al. observed in their studies that the average value of a critical Reynolds number for a helical pipe is about 2300, which is the same as that of a straight pipe. However, Re_{crit} depends on the torsion of the pipe; the minimum value was 800 for β = 1,3 and the maximum 2800 for β = 0,5. The transition of the flow for the helical pipe was not abrupt, but occurred gradually; consequently the Re_{crit} indicates the beginning of the turbulent flow causing the flow, to be fully turbulent around Re = 8000. The curvature has a stabilizing effect (increases Re_{crit} heavily) on the flow, whereas torsion shows a destabilizing effect.

Hence, the pressure losses calculated for the present heat transfer pipes using Equations (18) for laminar (Re < 2300) and (21) for turbulent flow (Re >2300), respectively, and compared to that of similar straight pipes. Results are presented in Chapter 7.1.2. The pressure loss per length of pipe L is calculated by

$$\frac{\Delta p}{L} = f\,\frac{\rho v^2}{2d_i} \qquad (22)$$

where ρ is the density of HTF and v the flow velocity. The friction factor for a straight pipe according to the Blasius equation for turbulent flow is

$$f_{s,T} = \frac{0{,}3164}{\mathrm{Re}^{0,25}} \tag{23}$$

5.3.3 Entropy generation in helical pipe

An inevitable problem met by helical pipes is that the heat transfer enhancement due to an increase in curvature is always achieved at the expense of an increase in friction loss. Ko (2006) studied the optimal curvature ratio δ in helical pipes by the thermodynamic second law based on the minimal entropy generation principle. The influence of the curvature ratio on entropy generation from frictional and heat transfer irreversibility were analyzed. It was discovered that the steady state entropy generation in helical coiled pipes is closely related to the Reynolds number and curvature ratio, but is relatively insensitive to the coiled pipe pitch. Ko studied steady state heat transfer with constant wall heat flux and surface temperature. This theory was applied to unsteady state heat transfer and the optimal curvature ratio for the current heat transfer pipes was calculated.

The basis of Ko's entropy generation calculations was to consider heat transfer rate and entropy generation per unit coil length. Entropy generation rate per unit length of pipe is defined by

$$\dot{S}'_{gen} = \dot{S}'_{gen,T} + \dot{S}'_{gen,p} \tag{24}$$

where $\dot{S}'_{gen,T}$ and $\dot{S}'_{gen,p}$ represents the unsteady state entropy generation through the irreversibility from heat transfer and pressure losses by fluid friction, respectively and are defined by

$$\dot{S}'_{gen,T} = \dot{S}'_{gen,T_{st}} + \frac{dS'_T}{dt} \tag{25}$$

$$\dot{S}'_{gen,p} = \dot{S}'_{gen,p_{st}} + \frac{dS'_p}{dt} \tag{26}$$

where $\dot{S}'_{gen,T_{st}}$ and $\dot{S}'_{gen,p_{st}}$ are the steady state entropy generation terms through heat transfer and pressure losses suggested by Ko and Ting (2005). The term dS'_T/dt represents the unsteady state entropy generation through heat transfer and is approximated by

$$\frac{dS'_T}{dt} \approx \frac{m_w c_{p,w} \ln\left(\frac{\overline{T}_w(t+\Delta t)}{\overline{T}_w(t)}\right)}{L\Delta t} \qquad (27)$$

where m_w is the mass of water in pipe, L the total length of curved pipe and $\overline{T}_w$ the average temperature of the water taken as a average from measured inlet and outlet temperatures.
The term $dS'_p/dt = -(V\gamma\ \Delta p/L/\Delta t)$, where V is the inner volume of the pipe, γ the heat expansion coefficient of water, represents the unsteady state entropy generation through pipe pressure losses, which in the case of constant flow rate has no importance. For example entropy generation through heat transfer irreversibility in certain situation (Eq. 27) is $1{,}4\cdot10^{-3}$ J/mK and $9{,}5\cdot10^{-6}$ J/mK through pressure losses respectively. The steady state entropy generation terms on the right side of Equations (25) and (26) are expressed as (Ko, 2005)

$$\dot{S}'_{gen,T_{st}} = \frac{\varphi'^2(t)}{\overline{T}_w^2(t)\pi Nu\lambda_w + \overline{T}_w(t)\varphi'(t)} \qquad (28)$$

$$\dot{S}'_{gen,p_{st}} = \frac{\dot{m}_w^3 f}{\overline{T}_w \rho_w^2 r_{p,i}^2 \pi^2} \qquad (29)$$

where λ_w is the thermal conductivity of water, φ' is the heat transfer rate per unit of pipe length (Eq. 4). *Nu*, *He*, *De* and *Re* are calculated from Equations (12), (13), (8) and (9).

5.4 Efficiency of heat exchangers

Effectiveness is used to compare various conventional heat exchangers with steady state heat transfer. The effectiveness, or heat transfer efficiency, is defined here with an equation

$$\varepsilon = \frac{\varphi}{\varphi_{\max}} = \frac{\left(T_{w,o} - T_{w,i}\right)}{\left(T_{w,o,\max} - T_{w,i}\right)} \tag{30}$$

where $T_{w,o}$ is the measured outlet temperature of the cooling water, $T_{w,i}$ the inlet temperature of the cooling water and $T_{w,o,\max}$ the theoretical maximum temperature of the outlet flow. This method is applied to the unsteady state heat transfer with a nonflowing PCM at the other side of the heat exchanger in order to have one criterion value, with which to compare the different brush heat exchangers. The heat transfer efficiency varies in every time step as ΔT_w varies. The theoretical maximum water outlet temperature has to be calculated with the following equation

$$T_{w,o,\max} = T_{s,o} - \left(T_{s,o} - T_{w,i}\right)\exp\left(\frac{-P_i L}{\dot{m} c_{p,w}}\alpha_i\right) \tag{31}$$

where $T_{s,o}$ is the outer surface temperature (the melting temperature of the PCM) of the heat transfer pipe, P_i the inner circumference of the pipe and α_i the heat transfer coefficient inside the pipe. The heat transfer coefficient is gained from the definition of the Nusselt number

$$Nu = \frac{\alpha_i d_i}{\lambda_w} \tag{32}$$

as the Nusselt number is first calculated from Equation (12).

6 EXPERIMENTAL SETUP AND PROCEDURES

Experiments were conducted with four brush heat exchangers. The first heat exchanger, the tank brush heat exchanger, was predesigned by Oy Hydrocell Ltd. and was used as a preliminary heat exchanger to examine the supercooling properties of SAT with metal contact and the overall test procedures. The other three, called tube brush heat exchangers, were manufactured by experience and ideas born with the experiments on tank brush heat exchangers.

Table 3. Information from experiments with different brush heat exchangers.

BHX	PCM	Mass of PCM (kg)	Re	Cooling method and HTF	Experiment no.
Tank	90% SAT 89% SAT +CMC	3.6	500-33000	Tap water	1-30
A	89% SAT +CMC	2.1	500-5000	Cooling device, water	31-62
B	90% SAT 89% SAT +CMC	2.3	500-5000	Cooling device, water	63-95
C	89% SAT +CMC	2.3	500-5000	Cooling device, water	96-118

Mainly, the PCM used in the BHXs contained 89 wt% of SAT, 1 wt% of CMC and 10 wt% of distilled water. Also, a few experiments without CMC were conducted. Temperature of the PCM in various locations, temperature of the outer surface of the container and the inlet and outlet temperatures of the heat transfer fluid (water) were measured. Table 3 summarizes the experimental settings done with the BHXs and it includes the failed experiments as well. Various Reynolds numbers for the HTF flow were used. The temperature of the heat transfer fluid in the tube brush heat exchanger experiments was mainly 20 ºC and the crystallization temperature of the sodium acetate trihydrate was

around 25 ºC. In addition, comparative experiments with different HTF temperatures were performed.

The test facility used in the experiments is shown in Figure 6. This system consisted of a heat storage unit with brush heat exchanger, feed heater, heat transfer fluid supply system, data requisition device and PC. Temperatures were measured with calibrated K-type thermocouple time intervals varying from 4 to 10 seconds. In addition, with the largest *Re* in tube brush heat exchangers, an exterior pump with a frequency changer was utilized. The mass flow of HTF was assessed with stopwatch and scale. Heat exchangers were insulated with a 50 mm mineral wool layer and aluminum foil. Tap water was used as HTF in the experiments with tank BHX; later cooling device Haake DC50 with distilled water as heat transfer fluid was employed.

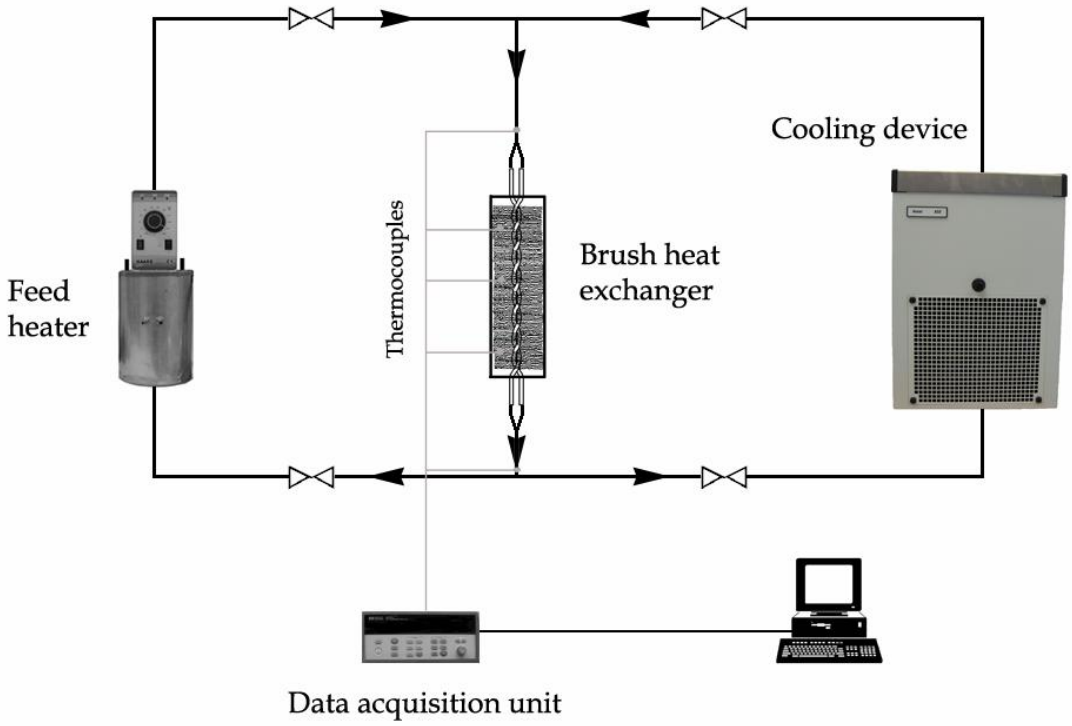

Figure 6. Schematic diagram of the experimental setup.

6.1 Experiments with tank brush heat exchanger

The first batch of PCM used with tank BHX (90 wt% SAT and 10 % extra water with total mass of 3,6 kg) was melted and poured into the heat exchanger container. Experiments were performed between 2007-11-22 and 2007-11-28. After the sixth thawing, the liquid PCM would crystallize no more, although it was once more heated to around 70 ºC. Phase segregation had occurred averting crystallization. Experiments were continued with small glass tubes (see Chapter 7.5.2).

Earlier tests with 2 wt% of CMC and 10 wt% of water made the PCM too jellylike to handle; accordingly the second batch of PCM was made of 89 wt% SAT, 1 wt% CMC and 10 wt% of distilled water.

With the new PCM batch, a total of 25 experiments were performed in the heat exchanger between 2007-01-15 and 2007-03-06. The PCM thermocouples (nos. 10–13 in Figure 7) were pushed from the top into the container and their exact location remained unknown. Most likely some, if not all, of the thermocouples were in contact with the metal brush filaments.

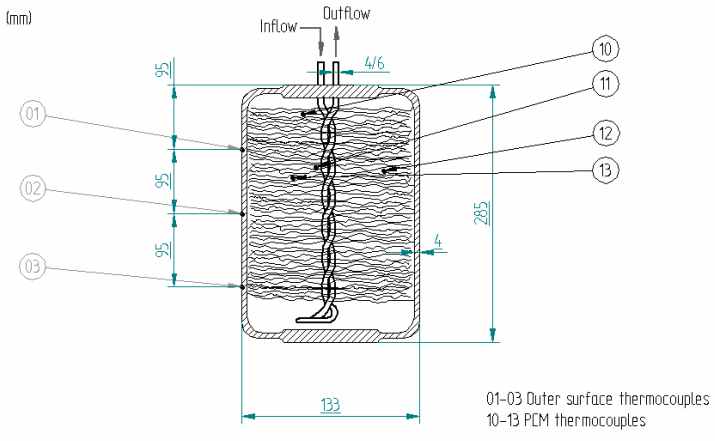

Figure 7. Schematic diagram of tank brush heat exchanger and the dimensions and locations of thermocouples. The exact locations of PCM thermocouples 10–13 were unknown.

6.2 Experiments with tube brush heat exchangers

Brush heat exchangers were installed in an acrylic tube and the ends sealed. Six thermocouples were inserted through the tube and glued properly. Thermocouples were positioned at three vertical levels, two at each level, and at two radial depths. The vertical distance of the thermocouples was 150 mm and the depths measured from the outside surface of the acrylic tube were 15 and 30 mm, respectively. In addition, three thermocouples were glued to the outer surface of the acrylic tube in three vertical positions. The brush heat exchanger with acrylic tube container with melted sodium acetate trihydrate is presented in Figure 8. A small gap (5 mm) between the acrylic tube inner surface and the brush filaments was left to ensure that the outer thermocouples were not in contact with the metallic brush filaments.

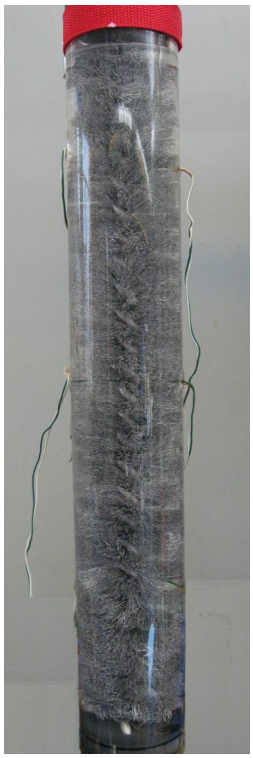

Figure 8. Brush heat exchanger with acrylic tube container and melted sodium acetate trihydrate.

6.2.1 Brush heat exchanger A

Between 2007-03-21 and 2007-04-17 a total of 20 freeze-thaw cycles were performed, resulting in only four successful measurements. Small but severe leaking problems prevented supercooling and PCM was removed from the container. A silicon gasket was extruded inside the container bottom to prevent the leaking and to fill the brushless space on the bottom. With a second batch of PCM, the silicon gasket completed only a few cycles before final break up.

The experiments with a new, somewhat shorter, BHX A were conducted between 2007-07-02 and 2007-07-10 with the result of 11 crystallization of the PCM. Untill the sixth crystallization, both the heat exchanger and the PCM worked satisfactorily. The seventh crystallization occurred spontaneously and the eighth spontaneously while cooling with water. After the eighth crystallization leakage was noticed, repairs were tried, but only with poor results. The following experiments suffered from the leakage, as crystallized particles outside the heat exchanger container prevented supercooling.

Figure 9 presents the dimensions of BHX A and locations of the K-type thermocouples. In distinction from the tank BHX experiments, heat transfer fluid was supplied with Haake DC 50 cooling apparatus. PCM's consistency was the same as in the first experiments (89 wt% SAT, 10 wt% water and 1 wt% CMC) with total mass of 2,1 kg.

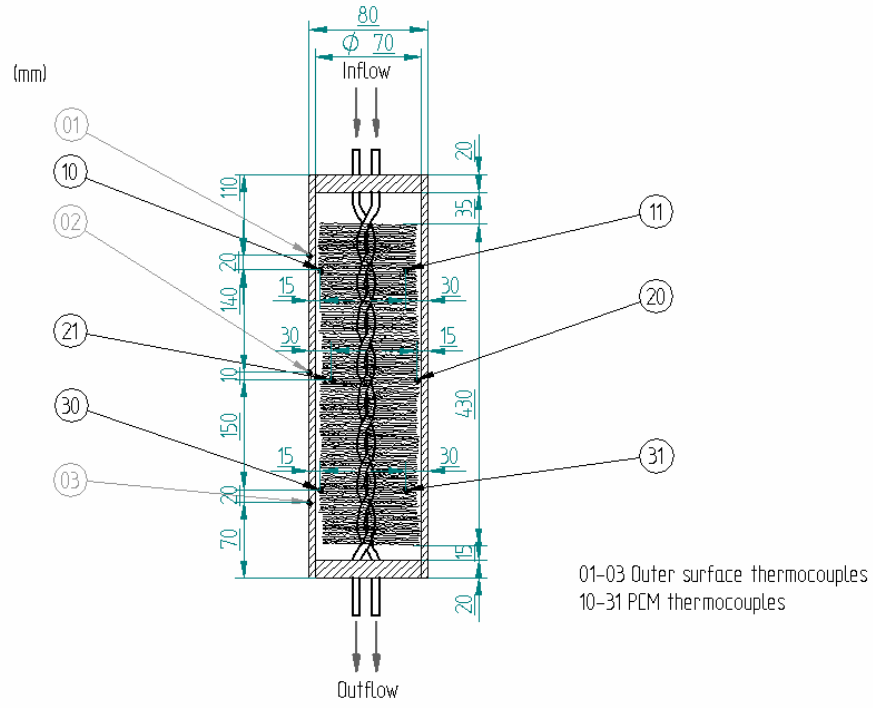

Figure 9. Schematic diagram of tube brush heat exchanger A; the dimensions and locations of thermocouples.

6.2.2 Brush heat exchanger B

With one batch of PCM, containing CMC, altogether 20 freeze-thaw cycles were completed between 2007-04-30 and 2007-05-23. Experiments with a second batch without CMC were performed between 2007-05-30 and 2007-06-04, yielding three succesful measurements. The purpose of the experiments without CMC was to discover if it has any affect on the power, recovered heat, peak crystallization temperature and gas formation (discussed in Chapter 7.5.4).

With the first batch of PCM, it was discerned that the PCM was more jellylike on top of the tube than in the bottom. Because of this, the third batch was melted and crystallized numerous times before inserting it into the heat exchanger. These experiments were performed 2007-06-07 – 2007-06-18 without insulation, to allow visual inspection of the PCM and the crystallization process. Degrees of supercooling in a total of eight

experiments were less than 15 ºC. Because of the lack of insulation and low supercooling, experiments were halted minutes after crystallization and no data was saved. Figure 10 shows the dimensions of the BHX and the locations of the thermocouples.

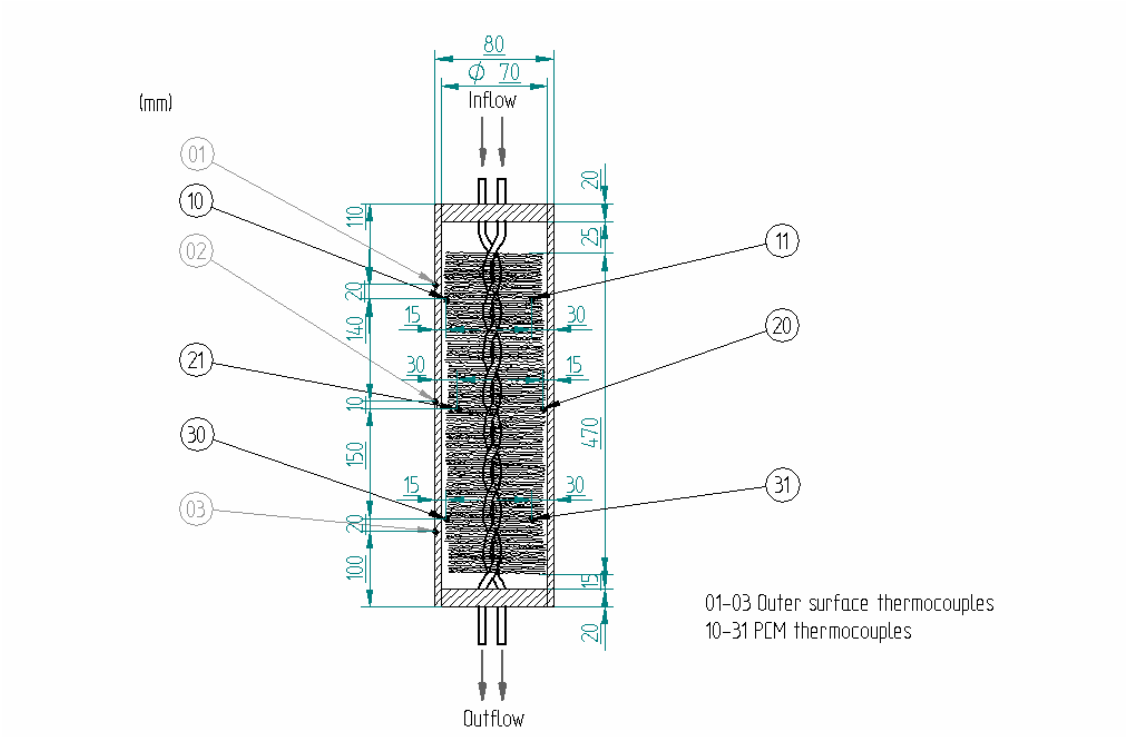

Figure 10. Schematic diagram of tube brush heat exchanger B; the dimensions and locations of thermocouples.

6.2.3 Brush heat exchanger C

In the period 2007-05-17 – 2007-06-20, a total of 24 cycles were performed with one batch of PCM containing 1 wt% of CMC and 10 wt% of water. Various degrees of supercooling and inlet water temperatures and velocities were used. Some leaking problems arose as thermal stresses bended the plastics, but that was successfully taken care of. BHX C's acrylic tube was 10 mm longer on the top than tube B, otherwise the lay-out was similar to that shown in Figure 10.

7 RESULTS AND DISCUSSION

7.1 Curved pipe flow characteristics

7.1.1 Heat transfer coefficient

In Chapter 5.3.1, various propositions for the Nusselt number for a curved pipe were presented. Figure 11 presents these correlations drawn for water with different Reynolds and Dean numbers, when curvature (d_i/D) = (4/12) mm and pitch b = 27,6 mm, as in the brush heat exchangers. The *Nu* for a straight pipe according to the Dittus-Boelter equation (*Re*>2300) was drawn for comparison as it is defined by

$$Nu = 0{,}023\,\mathrm{Re}^{0,8}\,\mathrm{Pr}^{0,4} \qquad (33)$$

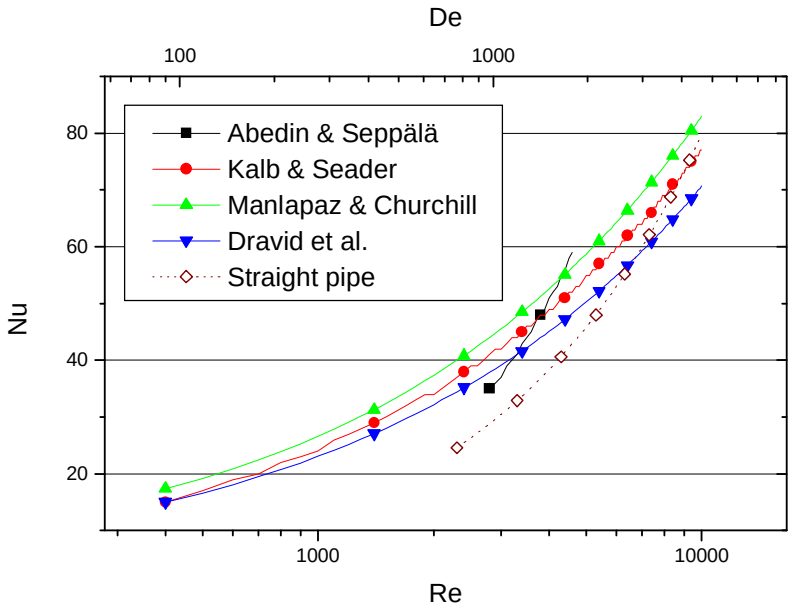

Figure 11. Various suggestions for Nusselt number in curved pipe heat transfer.

The modified Nusselt by Abedin and Seppälä is only valid in a small range of Reynolds numbers and is in good agreement with the other correlations. As *Re* increases, the correlation approaches that of a straight pipe. According to Figure 11, the correlation of

Kalb and Seader (Eq. 11) was chosen for calculating the heat transfer coefficient inside the helical pipes. Although the value might not be totally correct, for comparison of the different brush heat exchangers, it is an adequate approximation.

7.1.2 Pressure losses

The friction factor for flow in a helical pipe is calculated with Equations (21) and (18) for turbulent and laminar flows, respectively, and for a straight pipe with Equations (23) and (19). These friction factors and pressure losses for various Reynolds numbers are presented in Figure 12.

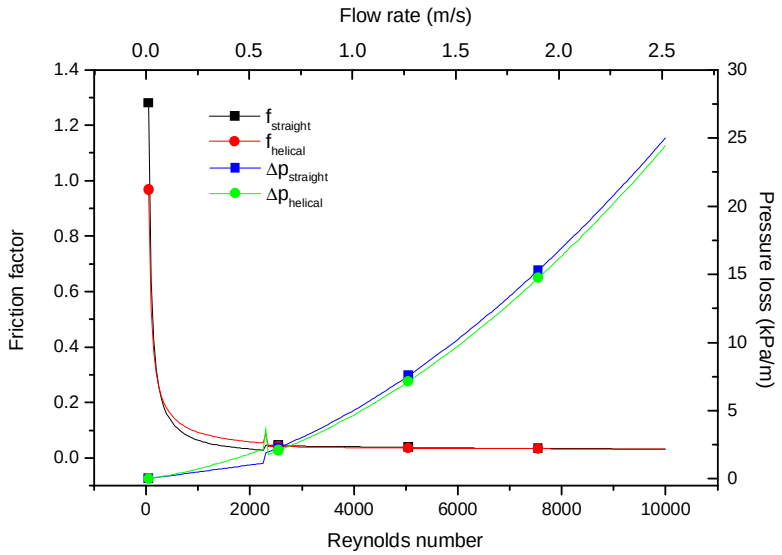

Figure 12. Friction factor and pressure losses for tube brush heat exchanger's heat transfer pipes.

The pressure loss in laminar flow (Re < 2300) is greater for the helical pipe than for a straight pipe, but becomes equal as the flow becomes turbulent; this was verified also by Yamamoto et al. (1995). The pressure loss (Eq. 22) in BHX's heat transfer pipes is very similar to that of the pressure loss a straight pipe.

7.1.3 Optimal curvature by minimizing entropy generation

The entropy generation equation (24) is a complex function of pipe diameter d, coil diameter D and pitch of coil b. The specific solution for the optimal curvature δ_{opt} is gained when pipe diameter and pitch was kept constant. Equation (24) was minimized with Excel's Solver by varying the coil diameter D for every time step in three measurements with different Re. Figures 13–15 illustrate the results. The optimal curvature for steady state heat transfer suggested by Ko, 2006 (Eqs. (28) and (29)) is also presented in the figures. The red line shows the proportional amount of heat recovered. The optimal curvature decreases steeply as the heat transfer rate drops and fluid friction begins to dominate the entropy generation.

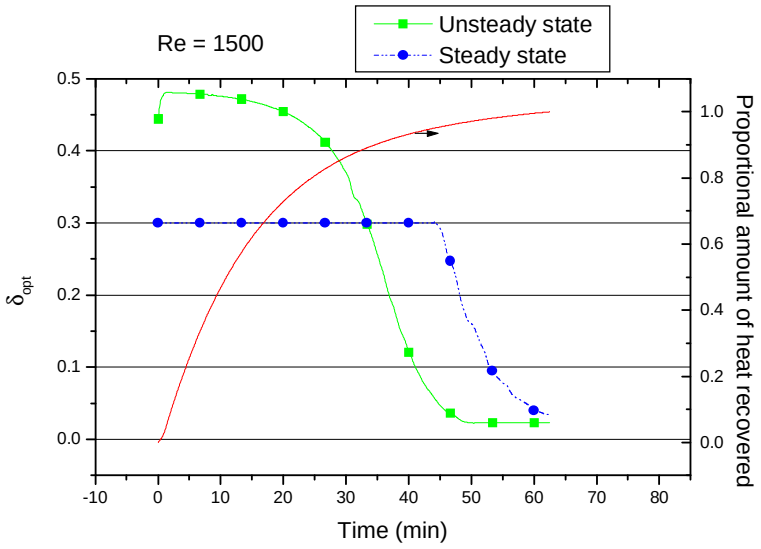

Figure 13. Optimal curvature of helical pipe in steady and unsteady state heat transfer when Re = 1500.

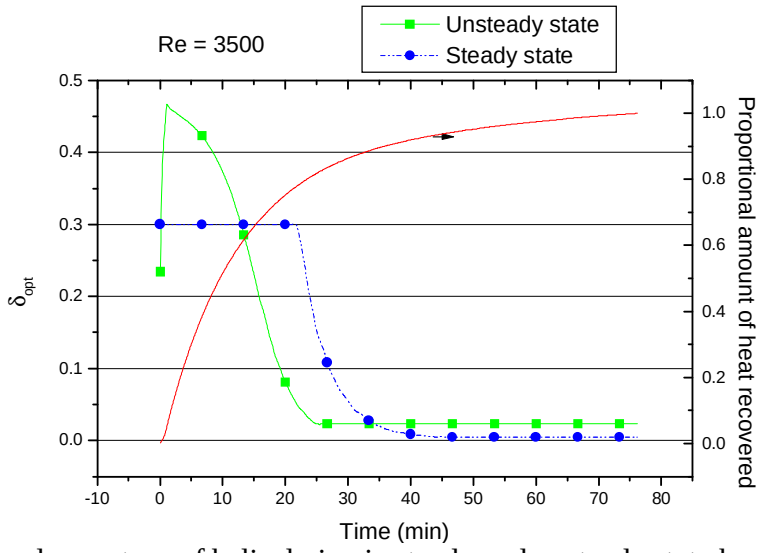

Figure 14. Optimal curvature of helical pipe in steady and unsteady state heat transfer when *Re* = 3500.

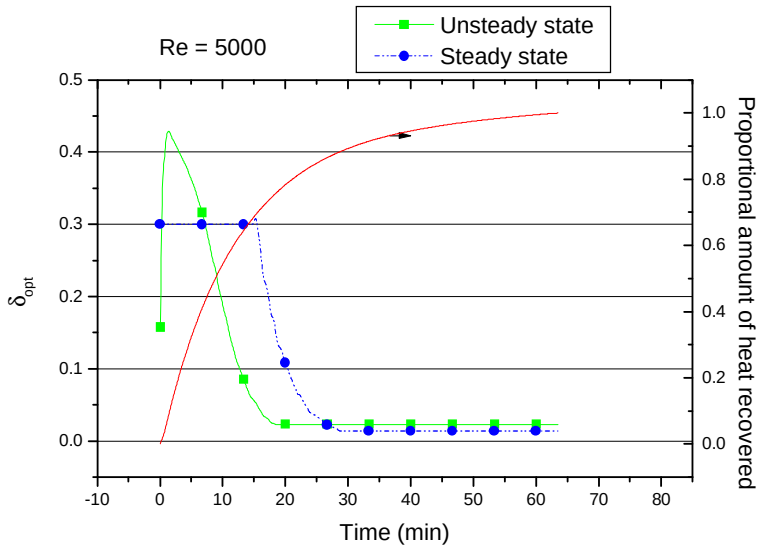

Figure 15. Optimal curvature of helical pipe in steady and unsteady state heat transfer when *Re* = 5000.

The curvature of current heat transfer pipes is 0,33, which is very close to the δ_{opt} for steady state case just after the crystallization. However, for smaller *Re* in unsteady state, heat transfer curvature should be increased, as over 80 % of the heat is recovered within the first 30 minutes and the average optimal curvature is around 0,47. Table 4 summarizes the optimal curvature for unsteady and steady state heat transfer. When *Re* = 3500, the optimal curvature for unsteady state and steady state are almost equal. As *Re* is further increased,

optimal curvature decreases because, with larger flow velocities, the friction irreversibility begins to dominate that of heat transfer irreversibility, and thus the curvature should be smaller (larger coil diameter) to resemble a straight pipe. The optimal *Re* for current heat transfer pipes is approximately 3500.

Table 4. Optimal curvature for steady state and unsteady state heat transfer calculated in a time period when 80 % of heat is recovered.

	Steady state	Unsteady state
Re	δ_{opt}	δ_{opt}
1500	0.3	0.47
3500	0.3	0.29
5000	0.27	0.2

7.2 Tank brush heat exchanger

A total of thirty measurements were conducted with the tank brush heat exchanger. Figure 16 represents the crystallizations in chronological order and describes whether the crystallization has been controlled and intentional or not. The crystallizations are classed in three categories: 1) the crystallization has occurred spontaneously while freely cooling in room temperature (red columns), 2) the crystallization has occurred spontaneously while cooling the SAT with water (green columns) and 3) the crystallization has occurred intentionally on adding a crystal on supercooled SAT while cooling with water (blue columns). The bottom of the column represents the temperature of the SAT when crystallization occurred and the top the peak temperature of the crystallized SAT. The results show that 30 % of the experiments worked intentionally, 20 % of the experiments the SAT had crystallized spontaneously and in 50 % of the experiments the crystallization occurred non-intentionally while cooling.

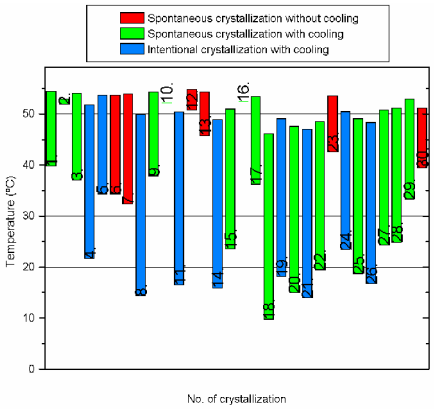

Figure 16. Crystallizations of SAT in tank brush heat exchanger in chronological order. Bottom of the column represents the beginning temperature of the crystallization and the top the peak crystallization temperature.

It can be noticed from Figure 16 that the trend is that more supercooled SAT has a lower crystallization temperature. Seppälä's studies (2007b) indicate a similar trend when sodium acetate trihydrate with CMC is used, but not with pure SAT and water mixtures. One explanation might be that the crystallization of highly supercooled SAT occurs so rapidly near heat transfer surfaces that the measurement time interval of the thermocouples is too long. Crystallized SAT on thermocouples would form a solid heat resistant and affect the peak temperature of crystallization. According to Seppälä (2007b), the temperature decrease of solid SAT near heat transfer surfaces is extreme, with several degrees in tenths of a second. Temperature, calculated power and recovered heat curves of all the experiments are presented in aggregate in Appendix A.

Accordingly, Figure 16 illustrates the main problem with the experiments of supercooled PCM: unwanted spontaneous crystallizations arise often extending the planned total time of the experiments.

7.2.1 Total results

In Figure 17, the calculated average power and recovered heat for the first 60 minutes after the crystallization of 17 applicable experimental data sets with various Reynolds numbers is

presented. For the reason that the measuring accuracy is limited, particularly for higher flow rates, a logarithmic curve is fitted into the data. Figure 18 shows the average temperature change of the HTF and, as can be seen for the higher flows, it is only a few tenths of a degree, which, compared to measurement accuracy of the thermocouples (± 1 ºC), inflicts a great marginal error. The recovered heat curve on figure 17 includes the potential sensible heat of the supercooled SAT and, accordingly, the recovered latent heats are lower.

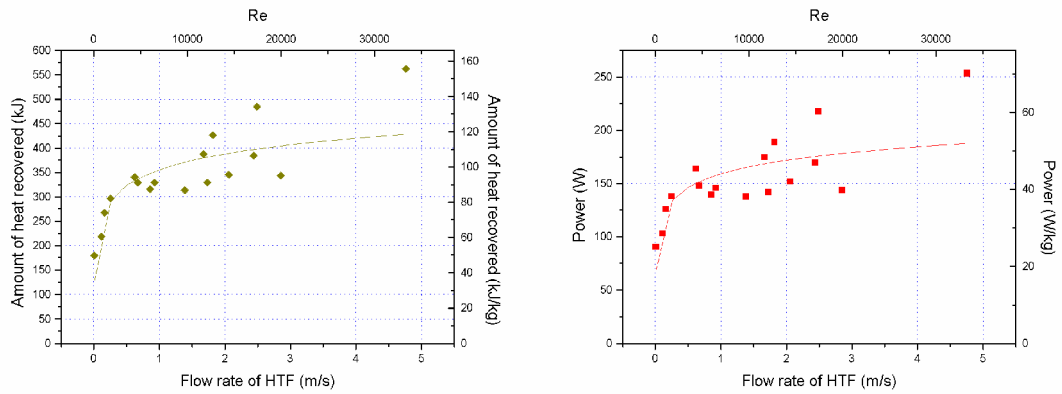

Figure 17. Amount of heat recovered and average heat transfer rate in tank heat exchanger within the first 60 minutes for various cooling water flow rates.

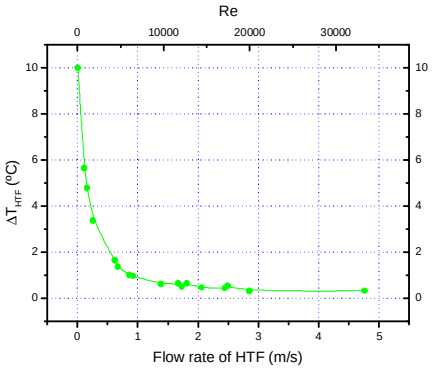

Figure 18. Average temperature variation of cooling water in tank heat exchanger within the first 60 minutes for various water flow rates.

It is clearly visible that, as the flow reaches Re_{cr} = 2300, power and the rate of recovered heat decreases heavily, but also that an increase of flow rate does not dramatically enhance the heat transfer after this point. Hence, it is proven that, with $Re > Re_{cr}$, the greater heat

transfer resistance exists between the phase change material and the brushes and not between the pipe surface and the cooling water. The cooling water temperature alteration has any practical value only for the smallest flow rates, pointing toward poor heat transfer efficiency and inappropriateness of the tank brush heat exchanger.

7.3 Tube brush heat exchanger

7.3.1 Temperature curves of supercooled crystallization

Sensible heat of the SAT has been lost because of supercooling but the largest proportion of charged thermal energy; the latent heat is released instantly on crystallization. Figure 19 shows the crystallization temperature curves as supercooled sodium acetate trihydrate undergoes phase change. The temperature of SAT rapidly rises to the peak crystallization temperature of 90 wt% SAT and immediately begins to cool.

Temperature rise measured with bottom thermocouples nos. 30 and 31 (Fig. 10) is normally higher than at the top of the tube (nos. 10 and 11). In addition, the temperature at the top cools faster. This suggests that the SAT solution has a larger amount of water present at the top of the tube than at the bottom. Temperatures also decrease faster near the cooling water tube, as expected. The surface temperature curves (01–03) are more round in shape and the bottom surface temperature varies with a higher temperature peak.

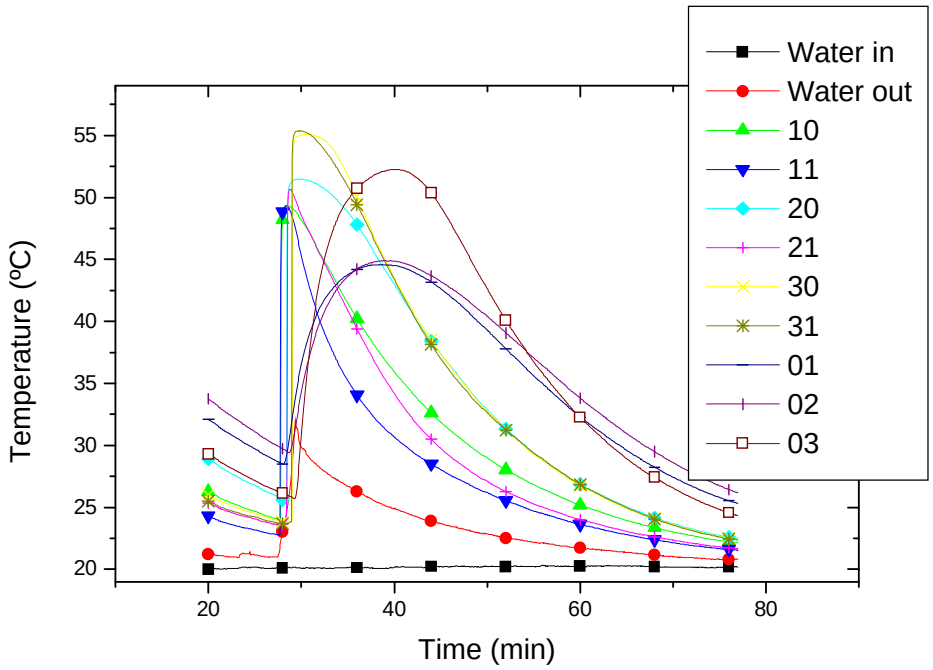

Figure 19. Supercooled crystallization temperature curves. (Experiment no. 53)

Another feature recognized throughout the experiments was the fact that in the first experiments, with a certain batch of PCM, the peak temperature difference between the top and the bottom was smaller than in later experiments. This implies that, regardless of the CMC, the phase segregation had begun to occur. One explanation might be that, either the heating had deteriorated the CMC leading to separation between the salt and the cellulose, or the mixing of CMC to SAT had not been sufficient.

7.3.2 Brush heat exchanger A

Figures 20 and 21 present the instantaneous output capacity and average output capacity, respectively. The curves in Figure 20 illustrate that the crystallization velocity of the supercooled sodium acetate trihydrate is high and so the release of the latent heat is rapid, yielding a high heat transfer rate peak at the beginning. As SAT crystallizes first on the heat transfer surfaces, immediately it begins to cool down, as reflected in the steep decrease of the output curve. The decrease is more conservative with smaller cooling water flow velocity (*Re* = 500) and the peak higher with larger Reynolds numbers.

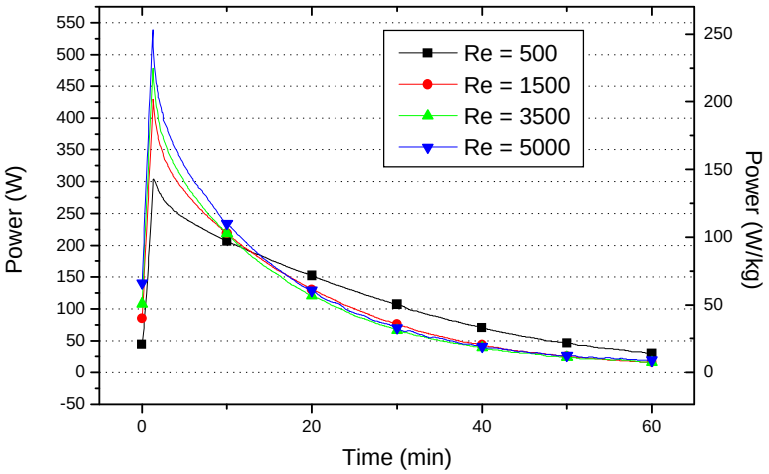

Figure 20. Heat transfer rate of brush heat exchanger A with various Reynolds numbers.

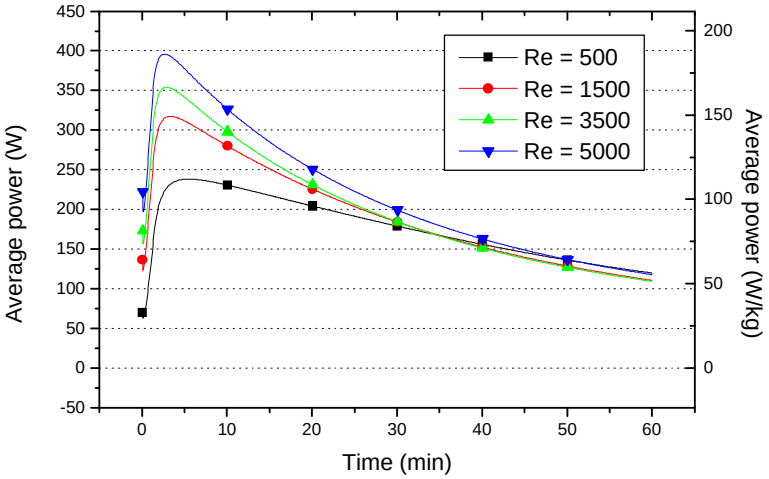

Figure 21. Average heat transfer rate of brush heat exchanger A with various Reynolds numbers.

Figure 22 presents the recovered latent heat for various Reynolds numbers. The heat is, however, recovered in a shorter time period with larger flow velocity. Appendix B represents all the temperature, power and heat curves gained from the experiments.

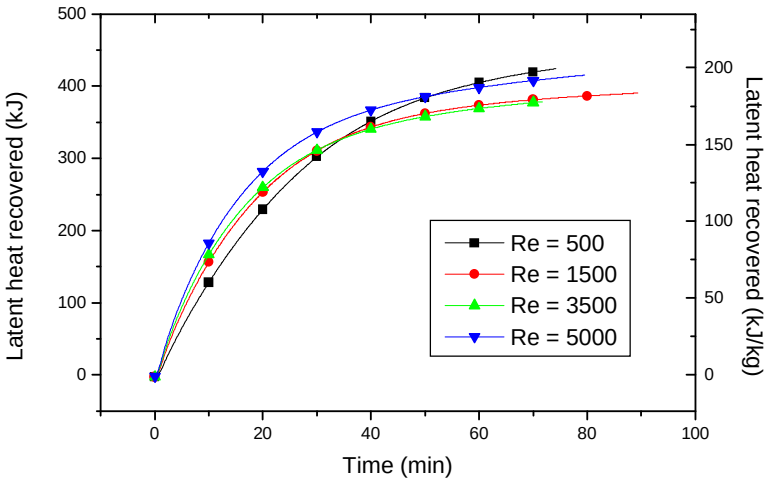

Figure 22. Recovered heat from brush heat exchanger A with various Reynolds numbers.

7.3.3 Brush heat exchanger B

The power curves in Figure 23 resemble the previous curves of the coarser BHX A with the difference of higher peak value. The average power in Figure 24 elucidates the differences between the different flow rates. Results show that the flow rate has a less significant affect on the output capacity after the flow is turbulent (*Re* > 2300).

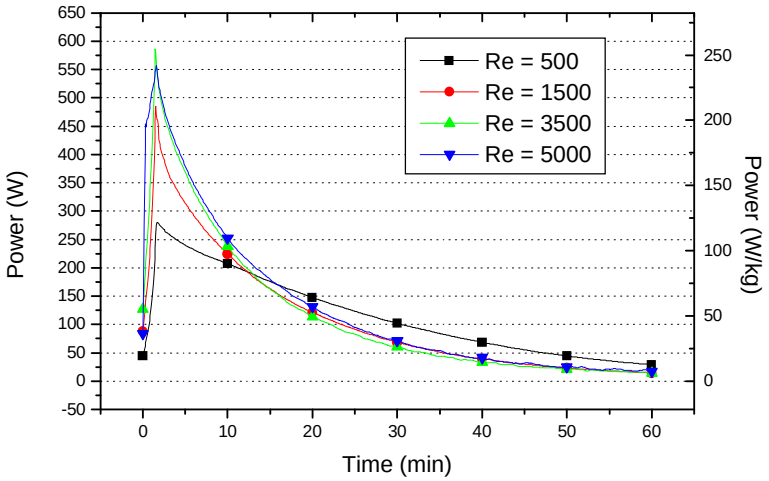

Figure 23. Output capacity of brush heat exchanger B with various Reynolds numbers.

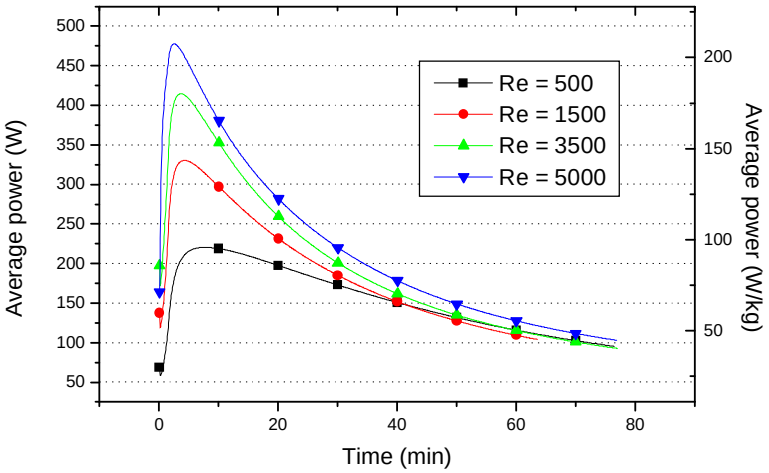

Figure 24. Average output capacity of brush heat exchanger B with various Reynolds numbers.

A rather large divergence can be noticed in Figure 25 showing the recovered latent heat; nonetheless, the differences can be explained by the reliability of the experiments. Recovered latent heat varies from 160 to 195 kJ/kg. All the experimental results of BHX B are illustrated in Appendix C.

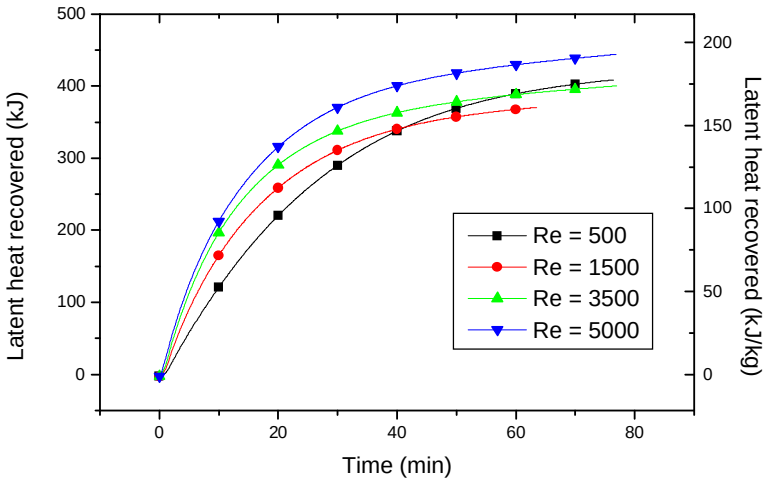

Figure 25. Recovered heat from brush heat exchanger B with various Reynolds numbers.

7.3.4 Brush heat exchanger C

The similarity with previously presented curves is noticeable in the output and average output curves of the thickest brush heat exchanger C presented in Figures 26 and 27.

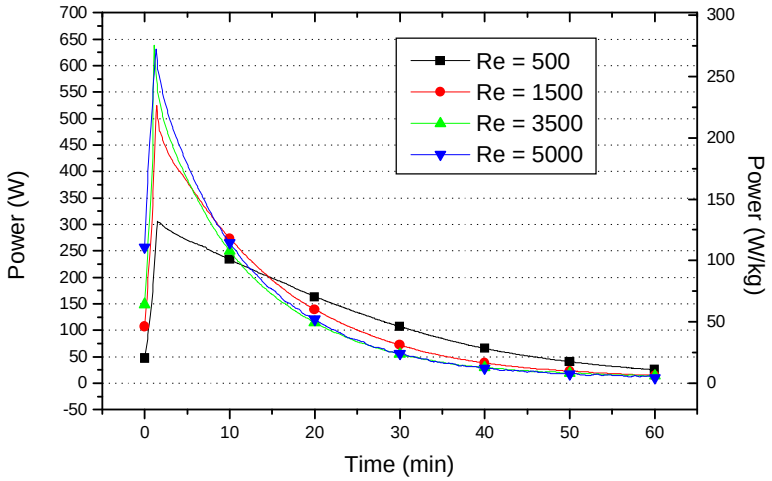

Figure 26. Output capacity of brush heat exchanger C with various Reynolds numbers.

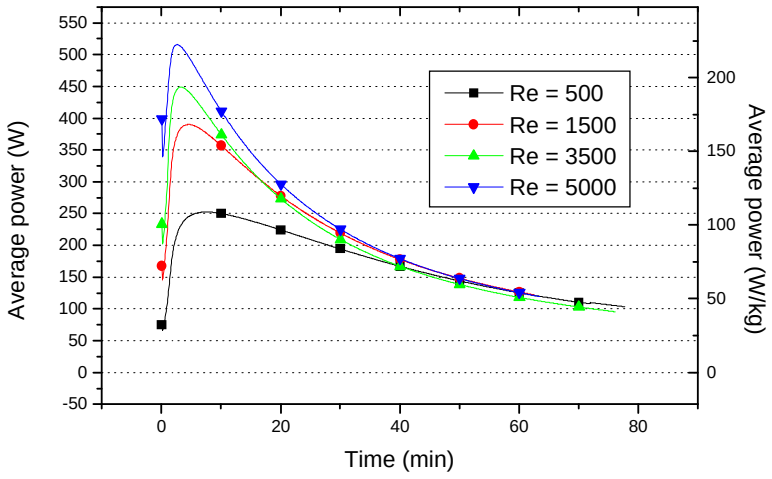

Figure 27. Average output capacity of brush heat exchanger C with various Reynolds number.

When the flow rate is increased 200 % (*Re* = 500 to *Re* = 1500) in the laminar zone (*Re* < 2300), the peak heat transfer rate increases 56 %. Accordingly, as flow rate is increased 133

% (from *Re* = 1500 to *Re* = 3500) from laminar flow to turbulent flow the peak heat transfer rate increases 15 %. A further increase from *Re* = 3500 to 5000 (43 %) accordingly increases the peak heat transfer rate also by 15 %.

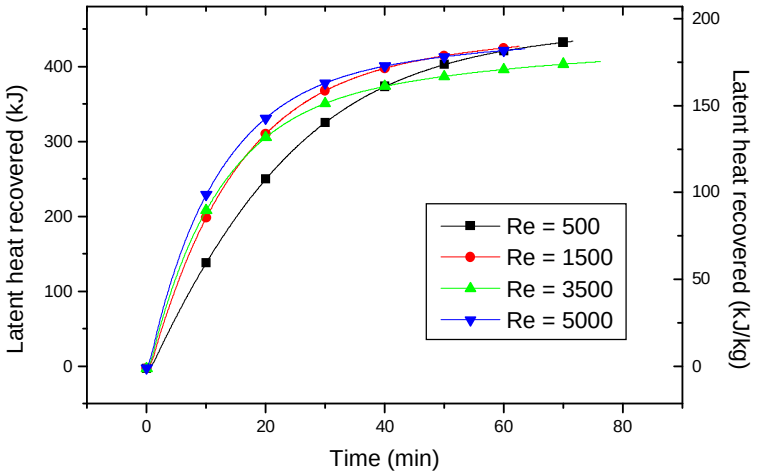

Figure 28. Latent heat recovered from brush heat exchanger C with various Reynolds numbers.

7.3.5 Effect of supercooling on output capacity

The effect that the degree of supercooling has on the output capacity was studied by varying the crystallization onset temperature, as water flow rate and water temperature were fixed. More sensible heat is recovered with a smaller degree of supercooling, but the effect on output capacity is minor, as Figure 28 shows. A difference of 5 ºC in the degree of supercooling affects only slightly the average output capacity. When the crystallization onset temperature was 40 ºC, the effect was larger. The degree of supercooling, however, has a lesser influence on the output capacities, but a stronger influence on the recovered heat.

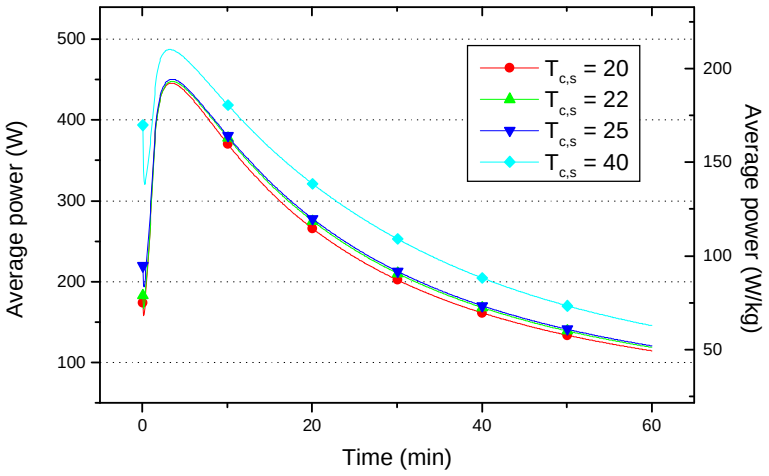

Figure 29. Average output capacities of brush heat exchanger C with various degrees of supercooling ($T_{c,s} = T_{sc}$).

7.3.6 Results of repeated experiments

Some experiments with brush heat exchanger C were repeated with identical measurement parameters. This would reveal the reliability of a single experiment, but also give a hint as to the stability[3] of the sodium acetate trihydrate, as other intervening experiments had done. Figure 30 shows the result of three experiments. It indicates good accuracy between measurements and good short-term stability of the PCM. Experimental details are found in Appendix D. However, the liquid SAT, CMC and water mixture removed from the brush heat exchanger after the final experiment (no. 118) was not clear anymore, but rather turbid and 'milky'.

[3] The capability to withstand the freeze-thaw cycles without any degradation in the thermal properties.

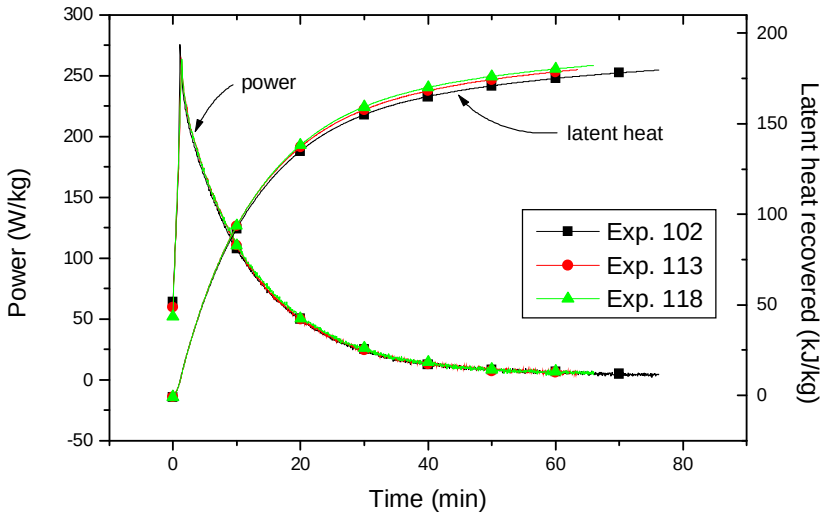

Figure 30. Three experiments with brush heat exchanger C with similar experimental settings.

7.4 Comparison of heat exchangers

7.4.1 Output capacity

The average power of the different heat exchangers for various Reynolds numbers is presented in Figures 31–34. Evidently, the efficiency of the tank brush heat exchanger is substantially lower than the tube brush heat exchangers. In a comparison of the tube BHXs, it is noticeable that, for smaller *Re*, the coarsest BHX A is the most efficient. For Reynolds number 1500 and above, the thickest BHX C has the best efficiency.

With smaller cooling flow rates, the heat transfer resistances between the PCM and the brushes and the brushes and heat transfer fluid are more equal than for higher flow rates when the heat transfer resistance between PCM and brushes begins to dominate. Therefore, the heat is released in a longer period of time with a smaller heat transfer rate. The denser brushes are more efficient for higher flow rates where heat transfer from PCM to brushes is the limiting factor.

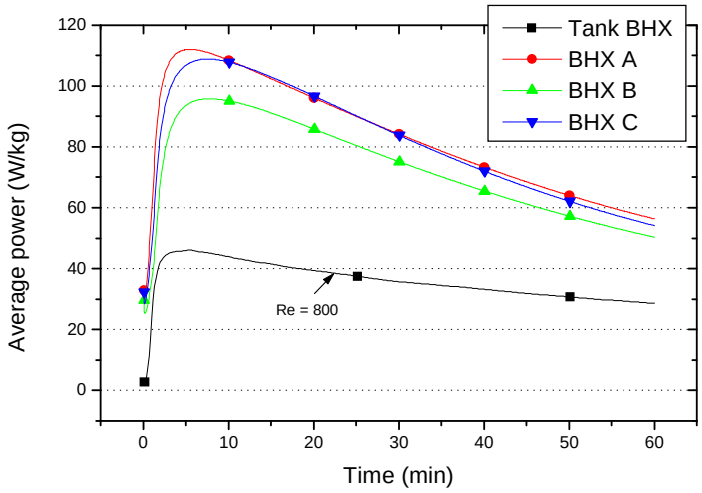

Figure 31. Average output capacity of the different brush heat exchangers when *Re* = 500

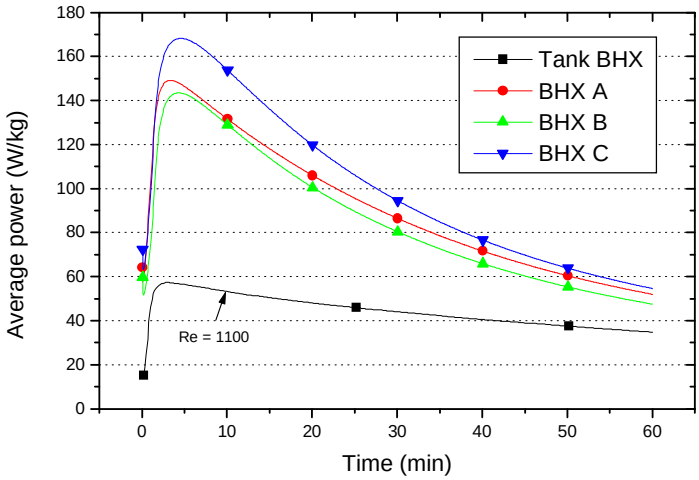

Figure 32. Average output capacity of the different brush heat exchangers when *Re* = 1500

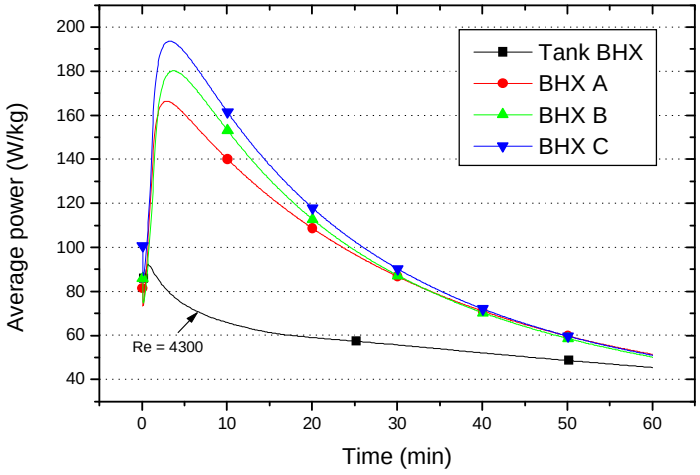

Figure 33. Average output capacity of the different brush heat exchangers when *Re* = 3500

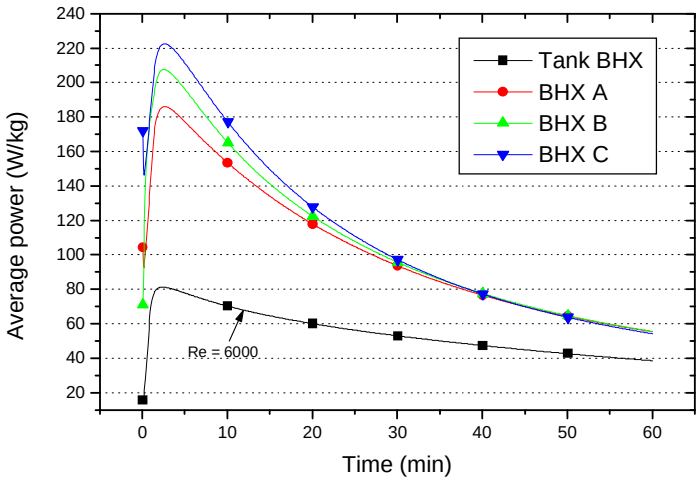

Figure 34. Average output capacity of the different brush heat exchangers when *Re* = 5000

7.4.2 Recovered heat

Figures 35–38 show the recovered latent heat of the tube brush heat exchangers with only minor discrepancies. The recovered latent heat from each of the heat exchangers after 60 minutes is around 175 kJ/kg, which, compared to the latent heat of 90-wt% sodium acetate trihydrate (190±10 kJ/kg), expresses that, first of all, most of the heat is recovered, and,

secondly, within the first hour. Naturally the heat is recovered in a shorter time with a higher cooling water flow rate.

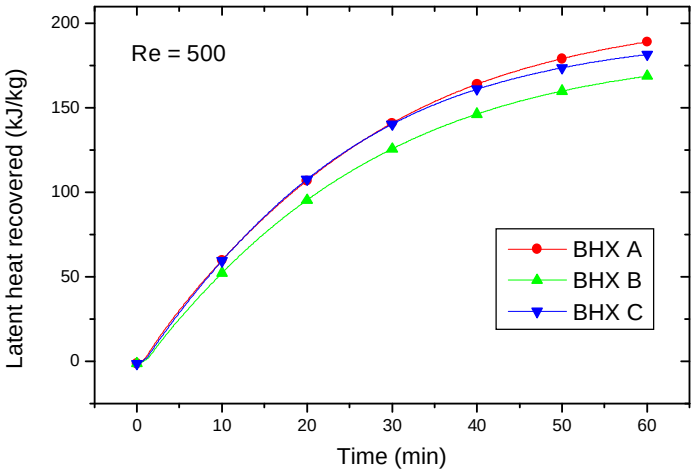

Figure 35. Latent heat recovered from the tube brush heat exchangers when *Re* = 500

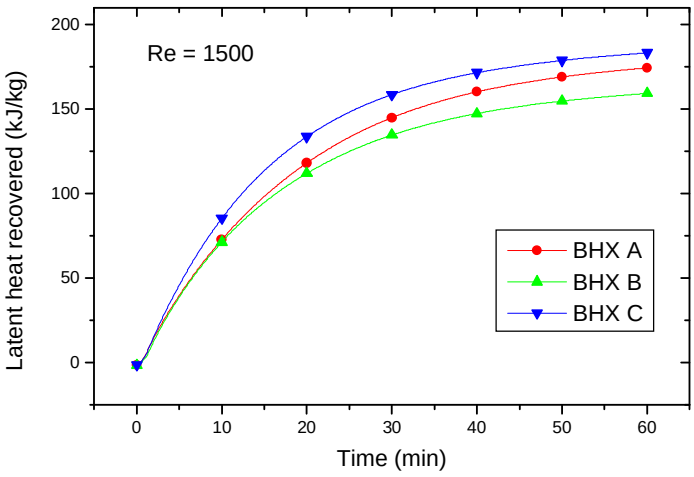

Figure 36. Latent heat recovered from the tube brush heat exchangers when *Re* = 1500

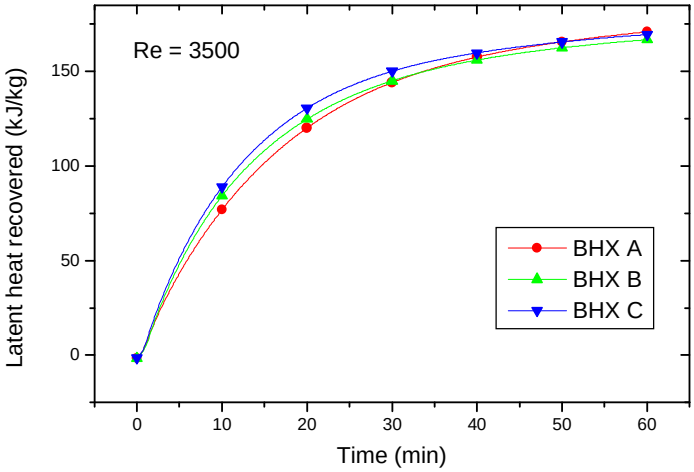

Figure 37. Latent heat recovered from the tube brush heat exchangers when *Re* = 3500

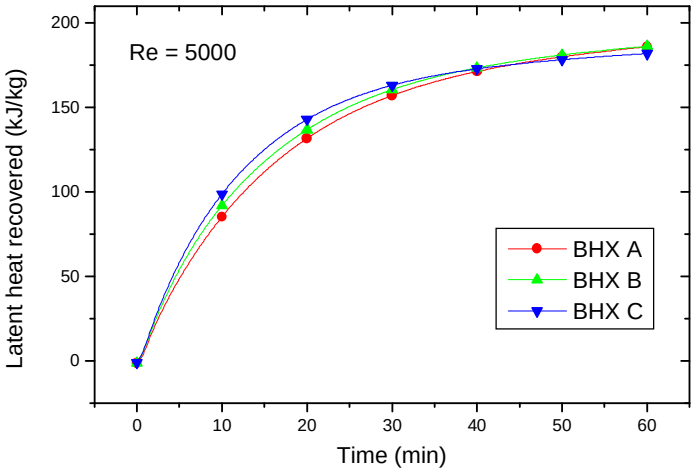

Figure 38. Latent heat recovered from the tube brush heat exchangers when *Re* = 5000

7.4.3 Heat transfer efficiency

To have one criterion factor for evaluation of the different brush heat exchangers; heat transfer efficiency was calculated with Equation (30). The pipe surface temperature was thought the same as the melting temperature of the PCM and, accordingly, $T_{w,o,max}$ by Eq. (31) presents the maximum water outlet temperature if crystallized SAT were not to act as

thermal resistance on heat transfer surfaces. Figure 39 presents the heat transfer efficiency for tube brush heat exchangers as a function of time. Due to the nature of the crystallization, the efficiency has a peak at the moment of crystallization and then it rapidly decreases. Table 5 reviews the calculated heat transfer efficiencies for the heat exchangers with various *Re*. The efficiencies of tank brush heat exchanger are only suggestive in nature because of differences in Reynolds numbers and the variations in inlet water temperature throughout the experiment.

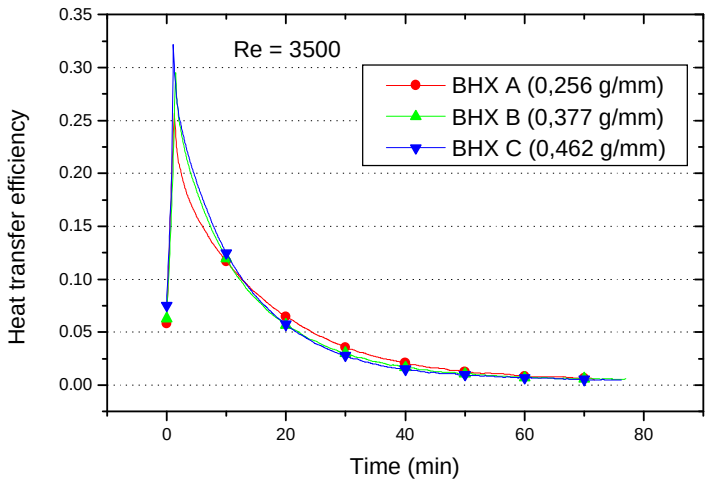

Figure 39. Heat transfer efficiency of the brush heat exchangers A–C.

Table 5. Average heat transfer efficiency when 80 % of total heat is recovered.

	Average heat transfer efficiency			
Re	Tank BHX	BHX A	BHX B	BHX C
500	~0,04	0,39	0,43	0,4
1500	-	0,18	0,18	0,23
3500	-	0,1	0,11	0,12
5000	~0,05	0,08	0,09	0,11

The average heat transfer efficiency was calculated when 80 % of the heat was recovered to make the small difference more visible. The efficiencies of the BHXs A–C are yet very analogous. Especially the small difference of efficiencies of BHX A and B, which have a larger difference of brush density (0,256–0,377 g/mm) than BHX C suggests that only after

a certain critical brush density does the increase of brush filaments begin to substantially affect the heat transfer.

7.5 Overall discussion

7.5.1 Charging

The given maximum operating temperature for the acrylic tubes was 80 ºC; therefore, sodium acetate trihydrate was melted with 84 ºC water flow. Besides, higher temperatures disintegrated the joints of the container more efficiently. Figure 40 presents temperature curves of the SAT when heated from the room temperature. The S-shape of the curves stems from the property of sodium acetate trihydrate to have a melting temperature range; in other words, the melting process begins at around 50 ºC and the medium is completely melted at 58 ºC.

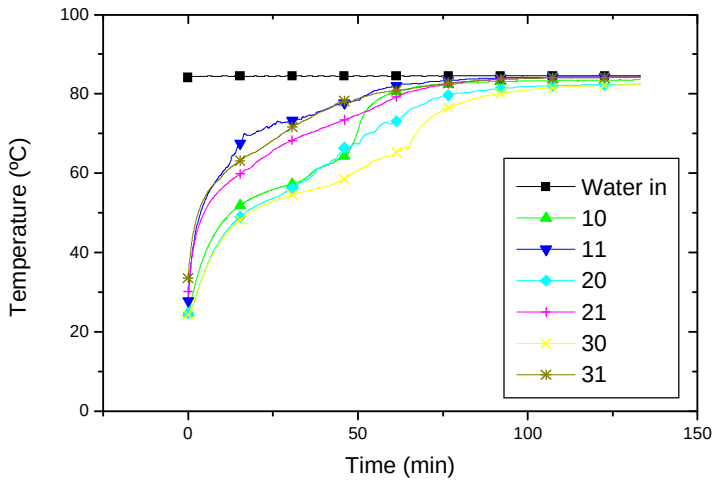

Figure 40. Melting curves of sodium acetate trihydrate (for the number of thermocouples, see Fig. 10)

Although, from the melting curves, it looks as if after 100 minutes the SAT has a temperature of above 80 ºC and so must have been completely melted, the brushless space with poor heat conductivity will require at least an extra hour to melt. Figure 41 shows the unmelted SAT ring at the bottom of the container. The melting time is drastically decreased

if a metal container is used instead of a plastic one. Another effect is that the melting is slower near the acrylic tube surface (thermocouples nos. 10, 20 and 30).

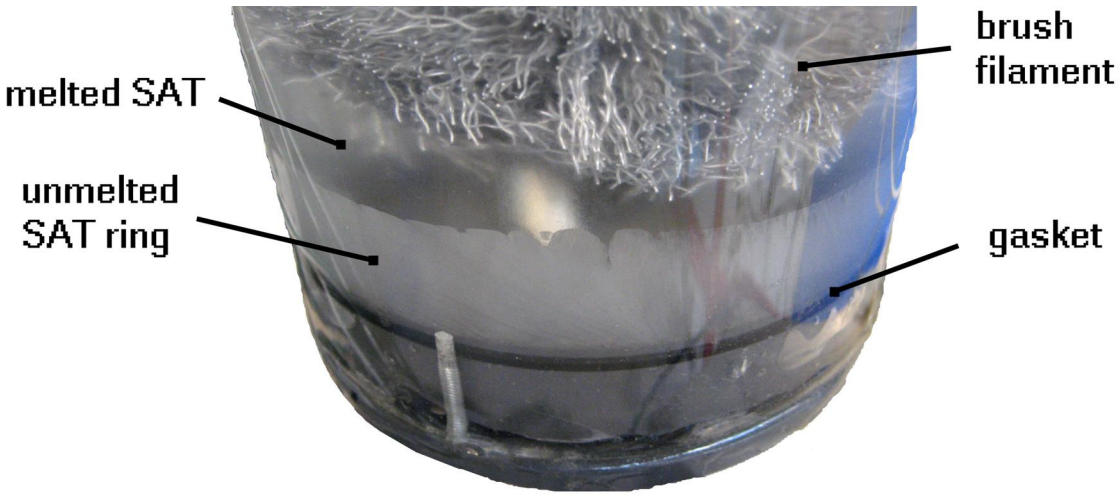

Figure 41. Unmelted SAT “ring” on the brushless space on the bottom of the acrylic container.

7.5.2 Crystallization experiments in glass vessels

After phase segregation had occurred, preventing any further crystallizations in the first experiment with the tank brush heat exchanger, the measurements were stopped and tests with SAT and CMC were started in 10 ml test tubes. Eleven different specimens were made, each specimen containing three tubes with the same concentration of PCM, CMC and water, yielding a total of 33 test tubes. The weight percent of CMC was either 0, 0,5 or 1, as the weight percent of distilled water varied from 0 to 20 with 5 percent increments. The samples were heated to around 80 ºC, cooled to room temperature (22 ºC) and crystallized 18 times to study the repeatability of the freeze-thaw process. Results showed no significant differences between samples. Every – even the pure SAT – sample crystallized and supercooled easily, while samples with CMC seemed to get better with more freeze-thaw processes because no white “foam” (anhydrous salt) while melting was formed. This was probably because the mixing of the CMC and PCM was imperfect and, after several tests the mixtures became more homogenous. One reason for the samples to

supercool effectively and maintain the metastable state for months was because of the small volume of the test tubes, which provided fewer locations for the nucleation to begin.

Consequently, experiments with larger glass bottles (vol. of 3 dm^3) filled with approximately 1,5 kg of 89 wt% of sodium acetate trihydrate, 1 wt% of CMC and 10 wt% of distilled water were performed. After first thawing, a gelatinous layer was formed at the surface of the melted PCM; the crystallization with salt particles was effortless. After the second thawing, only a few lumps of gelatinous PCM were noticed. After the third melting, the PCM was fluidic and bright. The bottle with liquid supercooled PCM was shaken vigorously, but no spontaneous crystallization occurred; yet, by adding salt crystal, crystallization was easy. PCM was melted yet again and placed into a freezer with a temperature of –15 ºC; it was stored there for a few days as supercooled liquid. Then it was stored at room temperature and the thermocouple pushed into the PCM to crystallize it. Measured peak temperature was 50 ºC.

The experiment conducted in the glass vessels, compared to the ones conducted in the brush heat exchangers, showed a significant difference in the stability of the supercooled metastable state and the degree of supercooling of SAT. In the glass vessels, SAT supercooled and maintained the metastable state with ease.

7.5.3 Velocity of crystallization front and supercooling

The rate of crystallization could be evaluated as thermocouples in different vertical positions registered the temperature rise of the phase change at different times. In the central experiments with T_{sc} = 25 ºC, $T_{w,i}$ = 20 ºC and with various *Re*, the velocity of crystallization was around 0,5 cm/s and varied diminutively between the different heat exchangers and Reynolds numbers. Similar rates were observed with the commercial heat pad supercooled to a room temperature.

The rate of crystallization with fixed mass flow rate of the coolant, but with various crystallization onset temperatures, showed that the rate varied from 0,2 cm/s to 0,6 cm/s as

onset temperature of crystallization varied form 50 ºC to 12 ºC, respectively. SAT without CMC seemed to have a slightly higher crystallization rate (0,5–0,6 cm/s), but, because of the exiguous number of the experiments, this is tentative.

The rate of cooling affecting the degree of supercooling was not studied specifically. Conclusions can be made from the tank brush heat exchanger experiments, but with desultory results. However, the general feeling when observing the measurements was that, with a higher rate of cooling, the supercooled SAT would crystallize easier with a lower degree of supercooling. This is controversial in relation to other studies (see, for example Choi et al., 1996), who state that a higher cooling rate increases the degree of supercooling.

7.5.4 Gas formation

Gas bubbles, not present in any of the experiments with glass vessels, appeared in heat exchange surfaces of melted PCM in acrylic tube brush heat exchangers (Figure 42). The diameter of the gas bubbles varied from <1 to 3 mm.

The reason for, and composition of, the gas remains unknown but container leakage and release of dissolved gases from the extra water have been suggested. Occasionally gas appeared only after a few melting cycles, so leaking was not the reason. The release of dissolved gases from the extra water is also unlikely, as gas was present even after several cycles.

Gas was formed with and without CMC; therefore, it could be that SAT reacted with the metals or plastics present. Whether the gas was air or something else (perhaps CO_2) remains a mystery, but, nevertheless, it will decrease the heat transfer rate in the liquid phase and as it forms cavities on crystallization. Kimura and Kai (1985) investigated the phase change stability of sodium acetate trihydrate thickened with $NaBr{\cdot}H_2O$ in heat cycle tests using vertical glass tubes. They reported that, after 1000 cycles, the anhydrous salt segregated on the bottom of the tube and “was full of bubbles”. The exact composition of the material was not analyzed.

Figure 42. Gas bubbles in liquid sodium acetate trihydrate and water mixture melted with brush heat exchanger.

7.5.5 Product development of supercooled latent heat storages

Evidently the structure of the tank brush heat exchanger with only one heat transfer pipe is unfavorable. A good aspect is that the sustainable aluminum tank made the melting more efficient. Therefore, the second stage of development heat exchangers had two heat transfer pipes. Their elongated shape was designed to avoid the heat exchanger being too small, as, if it were, proportional measurement errors would be larger. Moreover, the heat exchanger would be simple to manufacture and install into the rather small diameter acrylic tube container. A round container would not have sharp angles and joints for PCM to bore. A tubular container would also be more durable if pressure were to develop.

Despite careful design, major leakage problems were encountered on the bottom of the tube. Heat transfer pipe joints with the PVC cap, and the PVC cap itself, as well as the acrylic tube joints, disintegrated as plastics were exposed to cyclic thermal stresses. To retrieve the situation, silicon was extruded inside on the bottom of the tube. Perhaps because of the different thermal expansion coefficients of the materials, the gasket lasted

only a few freeze-thaw cycles. What is noticeable is that a diminutive spill is catastrophic for supercooled storage.

Minimizing brushless cavities and maximizing heat conduction of the container drastically shortens the melting time. If sodium acetate trihydrate is heated greatly above the melting point, thermal expansions must be taken into account. Complex geometries of containers, such as expansion tanks, should be avoided, as a single unmelted crystal in contact with the supercooled PCM can trigger premature crystallization. Melting and crystallizing the PCM a few times before inserting it into the heat exchanger improved the quality of the PCM; no stratification was noticed.

Designing of supercooled latent heat storage should start with the knowledge of temperature variation of the HTF. If a larger temperature rise is required, a smaller flow rate and coarse brushes should be exploited. If high output capacity is the goal, a denser brush and higher flow rate is the answer. Size and mass limits output capacity of heat storage, while pressure loss in heat transfer pipes has an effect on the overall efficiency of the system.

7.6 Measurement analysis

Error of calculated quantities through human accuracy and the accuracy of measuring instruments is evaluated. The repeated experiments showed that the reproducibility of the experiments is sufficient. The maximal relative error is estimated by adding the relative errors of quantities that it is formed by. Thus, relative error for output capacity is defined by

$$\frac{\Delta\varphi}{\varphi} = \frac{\Delta\dot{m}}{\dot{m}} + \frac{\Delta T_{w,o}}{T_{w,o}} + \frac{\Delta T_{w,i}}{T_{w,i}} \qquad (34)$$

where $\Delta\dot{m}$ is the maximal error of mass flow rate, $\Delta T_{w,o}$ and $\Delta T_{w,i}$ are the maximal temperature errors of inlet and outlet flows, respectively. The mass of water was measured with digital scale of accuracy ± 0,1 g (Δm) and the lapsed time with a stopwatch. The error

in time measuring (Δt) was estimated to be ± 0,5 s. The measured masses varied from 30 to 200 grams and corresponding times from 5 to 10 s. Consequently, the maximal relative error in mass flow rate can be calculated

$$\frac{\Delta \dot{m}}{\dot{m}} = \frac{\Delta m}{m} + \frac{\Delta t}{t} = \frac{0,1}{30} + \frac{0,5}{5} = 0,1033 \qquad (35)$$

Accuracy of thermocouples was ± 1 ºC and, as minimal water temperature in most experiments was 20 ºC, the maximum relative error of temperature measurement was 5 %. Therefore, the relative error of output capacity is given by

$$\frac{\Delta \varphi}{\varphi} = \left(\frac{0,1g}{30g} + \frac{0,5s}{5s} + \frac{1^{o}C}{20^{o}C} + \frac{1^{o}C}{20^{o}C} \right) \cdot 100 = 20,3\% \qquad (36)$$

The greatest error is due to the inaccuracy of mass flow rate, but the nature of the error is systematic, so it has a similar effect on every measurement. One must take cognizance of the fact that a slight error in PCM total mass and minor heat losses through the insulation exist.

8 SUMMARY

Waste heat of internal combustion engines could be stored in latent heat storage and discharged for the purpose of preventing negative factors related to cold starting. Supercooled PCM stores the energy without losses and the heat can be released when desired. The large conductance of the brush heat exchangers enhances the heat transfer rate from PCM of poor conductivity. The supercooling phenomena of sodium acetate trihydrate were investigated in brush heat exchangers to reveal the heat transfer rates, recovered latent heat and repeatability of the freeze-thaw cycles.

Controlling the supercooling by preventing premature spontaneous crystallization was the biggest challenge met by these experiments. The unpredictability of supercooling phenomenon was evidently discovered. Thickening agent CMC significantly improved the amount of freeze-thaw cycles that SAT could undergo without phase segregation but did not completely prevent it. Supercooling and the stability of the supercooled state were easier to attain in the glass vessels than in the brush heat exchangers. Besides, leaking problem due to a plastic PCM container made the experiments substantially harder to execute.

A tank brush heat exchanger, with one heat transfer pipe twined around itself, was considerably less efficient compared to the tube brush heat exchangers, whose differences in efficiency between themselves were minor. In tube brush heat exchangers, nearly all of the latent heat was recovered. A coarser brush was found to be more advantageousness for longer periods of heat discharge. If rapid heat discharge (higher heat transfer rate) is required, denser brushes are more suitable instead. Secondary water can be used to balance the heat transfer rate between the latent heat storage and the heat sink. Melting time was not affected by the brush density, but brushless volumes have to be minimized to ensure efficient charging of the latent heat storage. In addition, thermal expansion of the PCM has to be taken into account. The origins of formed gas in melted SAT requires further investigation as it impairs the heat transfer rate. Stratification of CMC and SAT was noticed in a vertical tubular container.

Reliable PCM with good supercooling ability and a sufficient nucleation barrier to prevent spontaneous crystallization, and yet permit external triggering of crystallization, are required. Small specific heat capacity of supercooling PCM is desirable as the theoretical minimum supercooled temperature decreases (Eq. 3) and because it does not affect the latent heat recovered. Long-term stability of thermal properties must be adequate for an economic lifespan.

Flow characteristics in curved pipes with large curvature were discussed. Several correlations for Nusselt numbers were presented and calculations for small diameter pipes were made. Heat transfer efficiency was better in curved pipes (with small diameter) than in straight pipe with small coolant flow rates, but, as flow velocity increased, the Nusselt numbers became similar. The optimal curvature of a curved pipe for unsteady state heat transfer was evaluated when stationary PCM was on the other side of the pipe by minimizing the entropy generation through heat transfer and flow friction irreversibilities, respectively.

The brush heat exchanger appeared to be efficient for latent heat recovery, but with the lack of comparative studies, no final conclusion can be made. Investigations with substantially coarse and dense brushes will probably reveal more distinctively the differences in heat transfer rates and will perhaps hint toward optimum brush density.

REFERENCES

Abedin, MD., Joynal. 2004. Experimental study of heat transfer coefficient in corrugated plate, curved and rough tubes of heat exchangers at low Reynolds number. Master's Thesis. Helsinki University of Technology, Department of Mechanical Engineering. Espoo, Finland. 80 p.

Angell, C.A. 1982. Supercooled water in Water A Comprehensive Treatise (ed. Franks, F.). Plenum Press. New York.

Araki, N., Futamura, M., Makino, A., Shibata, H. 1995. Measurements of Thermophysical Properties of Sodium Acetate Hydrate. International Journal of Thermophysics. Vol. 16. No. 6. P. 1455–1466

Arrhenius, G., Goldstein, M., Moore, C. 1982. Latent heat storage and supply system and method. United States Patent 4503838. P. 8.

Cabeza, L.F., Roca, J., Nogués, M., Mehling, H., Hiebler, S. 2002. Immersion corrosion tests on metal-salt hydrate pairs used for latent heat storage in the 48 to 58 ºC temperature range. Materials and Corrosion. Vol. 53. P. 902-907

Cabeza, L.F., Svensson, G., Hiebler, S., Mehling, M. 2003. Thermal performance of sodium acetate trihydrate thickened with different materials as phase change energy storage material. Applied Thermal Engineering. Vol. 23. P.1697–1704.

Callister, W.D., Jr. 2003. Material Science and Engineering An Introduction. 6th ed. USA. John Wiley & Sons. ISBN 0-471-22471-5

Chen, W.H., Jan, R. 1992. The characteristics of laminar flow in helical circular pipe. Journal of Fluid Mechanics. Vol. 244. P. 241–256.

Choi, J.C., Kim, S.D., Han, G.Y. 1996. Heat transfer characteristics in low-temperature latent heat storage systems using salt-hydrates at heat recovery stage. Solar Energy Materials and Solar Cells. Vol. 40. P. 71–78

Debenedetti P.G. 1996. Metasable Liquids: Concepts and Principles. Chichester: United Kingdom: Princeton University Press. P. 411. ISBN 0-691-08595-1.

Ettouney, H.M., Alatiqi, I., Al-Sahali, M., Al-Ali, S.A. 2004. Heat transfer enhancement by metal screens and metal spheres in phase change energy storage systems. Renewable Energy. Vol. 29. P. 841–860.

Farrell, A.J., Norton, B., Kennedy, D.M. 2006. Corrosive effects of salt hydrate phase change materials used with aluminium and copper. Journal of Materials Processing Technology. Vol. 175. P. 198–205.

Fukai, J., Kanou, M., Kodama, Y., Miyatake, O. 2000. Thermal conductivity enhancement of energy storage media using carbon fibers. Energy Conversion & Management. Vol. 41. P. 1543–1556.

Germano, M. 1989. The Dean equation extended to helical pipe flow. Journal of Fluid Mechanics. Vol. 203. P. 289–305.

Gök, Ö., Yilmaz, M.Ö, Paksoy, H.Ö. Stabilization of Glauber's salt for latent heat storage. http://intraweb.stockton.edu/eyos/energy_studies/content/docs/FINAL_PAPERS/4B-4.pdf

Häggblom, S. 2002. Experimental and Theoretical Analysis of the Usage of Brush Heat Exchangers in Heat Recovery and Cooling Systems in Air-Conditioning. Master's Thesis. Helsinki University of Technology. Department of Mechanical Engineering. Espoo, Finland. P. 84 (in Finnish)

Hamada, Y., Ohtsu, W., Fukai, J. 2003. Thermal response in thermal energy storage material around heat transfer tubes: effect of additives on heat transfer rates. Solar Energy. Vol. 75. P. 317–328.

Hamada, Y., Ohtsu, W., Fukai, J., Morozumi Y., Miyatake, O. 2005. Anisotropic heat transfer in composites based on high-thermal conductive carbon fibers. Energy. Vol. 30. P. 221–233.

Heinz, A., Streicher, W. Application of phase change materials and PCM-slurries for thermal energy storage.
http://intraweb.stockton.edu/eyos/energy_studies/content/docs/FINAL_PAPERS/4B-4.pdf

Kamimoto, M., Abe, Y., Sawata, S., Tani, T., Ozawa, T. 1985. Latent heat storage unit using form-stable high density polyethylene for solar thermal applications. Proceedings of the International Symposium on Thermal Application of Solar Energy. Hakone, Japan.

Kauranen P. 1989. Thermoanalyse of heat storage materials. Helsinki University of Technology, Department of Engineering Physics and Mathematics. Espoo, Finland. P.77. ISBN 951-22-0053-8.

Kimura, H., Kai, J. 1985. Phase change stability of sodium acetate trihydrate and its mixtures. Solar Energy. Vol. 35. No. 6. P. 527–534.

Ko, T.H, Ting, K. 2005. Entropy generation and thermodynamic optimization of fully developed laminar convection in a helical coil. International Communications in Heat and Mass Transfer. Vol. 32. P.214–223.

Ko, T.H. 2006. Thermodynamic analysis of optimal curvature ratio for fully developed laminar forced convection in a helical coiled tube with uniform heat flux. International Journal of Thermal Sciences. Vol. 45. P. 729–737.

Lamberg, P., Lehtiniemi, R., Henell, H-M. 2004. Numerical and experimental investigation of melting and freezing processes in phase change material storage. International Journal of Thermal Sciences. Vol. 43. P. 277–287.

Lane, G.A. 1986. Solar heat storage: Latent heat materials Vol. II. Boca Raton, Florida, CRC Press. 235 p. ISBN 0-8493-6586-4.

Mettawee, E.-B.S., Assassa, G.M.R. 2007. Thermal conductivity enhancement in a latent heat storage system. Solar Energy. Doi:10.1016/j.solener.2006.11.009.

Mullin, J.W., 2001. Crystallization. 4th ed. Oxford United Kingdom: Biddles Ltd. P. 594. ISBN 0-7506-4833.

Naphon, P., Wongwises, S. 2004. A review of flow and heat transfer characteristics in curved tubes. Renewable and Sustainable Energy Reviews. Vol. 10. P. 463–490.

Peippo, K. 1989. Faasimuutosvaraston termodynaamiset perusmekanismit ja energiasovelluksia. Helsinki University of Technology, Department of Engineering Physics and Mathematics. Espoo, Finland. P.81. ISBN 951-22-0054-6.

Sandness, B., Rekstad J. 2006. Supercooling salt hydrates: Stored enthalpy as a function of temperature. Solar Energy Vol. 80. P. 616–625.

Seppälä A., 2007a. Natriumasetaattitrihydraatin säilyminen alijäähtyneenä sekä kiteytymislämpötilan riippuvuus veden määrästä. PCM accumulator study report. Helsinki University of Technology, Department of Mechanical Engineering. P. 6.

Seppälä A., 2007b. Natriumasetaattitrihydraatin lämpötilajakauman kehittyminen alijäähtyneestä tilasta käynnistyvässä kiteytyksessä. PCM accumulator study report Helsinki University of Technology, Department of Mechanical Engineering. P. 14.

Seppälä A., 2007c. PCM accumulator study report. Helsinki University of Technology, Department of Mechanical Engineering.

Sharma, S.K., Jotshi, C.K. and Kumar, S. 1990. Thermal stability of sodium salt hydrates for solar energy storage applications. Solar Energy. Vol. 45. P. 177–181.

Shaukat, A. 2000. Pressure drop correlations for flow through regular helical coil tubes. Fluid Dynamics Research. Vol. 28. P. 295–310.

Stritih, U. 2004. An experimental study of enhanced heat transfer in rectangular PCM thermal storage. International Journal of Heat and Mass Transfer. Vol. 47. P. 2841–2847.

Tamme, R. 1984. Behaviour of sodium acetate trihydrate in a dynamic latent heat storage system. AIAA 19th Thermophysics Conference. June 25-28. Colorado.

Vasiliev, L.L., Burak, V.S., Kulakov, A.G., Mishkinis, D.A., Bohan, P.V. 2000. Latent heat storage modules for preheating internal combustion engines: application to a bus petrol engine. Applied Thermal Engineering. Vol. 20. P. 913–923.

Wada, T., Yamamoto, R., Matsuo, Y. 1984. Heat storage capacity of sodium acetate trihydrate during thermal cycling. Solar Energy. Vol. 33. P. 373–375.

Watson, W.K.R. 1973. Heat transfer system employing supercooled fluids. United States Patent 3952519. P. 9.

Yamamoto, K. 2006. Visualization of the flow in a helical pipe. Fluid Dynamics Research. Vol. 30. P. 251–267.

Yamamoto, K., Akita, T., Ikeuchi H., Kita, Y. 1995. Experimental study of the flow in a helical circular tube. Fluid Dynamics Research. Vol. 16. P. 237–249.

Yanase, S., Goto, N., Yamamoto K. 1989. Dual solutions of a flow through a curved tube. Fluid Dynamics Research. Vol. 5. No. 3. P. 191–201.

APPENDIX A

Experiments with aluminum the tank brush heat exchanger resulted in a total of 30 measurements with two batches of PCM. The results with measured crystallization temperatures, calculated average output capacities and recovered heat are presented in Table A1. Output capacity and recovered heat are computed within the first hour of crystallization. Figures A1–A8 present the temperature, power and heat curves of some of the experiments. The sensible heat is not reduced from the figures presenting recovered heat; therefore, the amount of heat recovered is dependent on the crystallization temperature (T_{sc}). The experiment numbers in bold refers to the intentionally crystallized experiments.

Table A1. Experiments with tank brush heat exchanger.

Experiment no.	Composition of PCM	PCM mass (kg)	T_{sc} (°C)	$T_{c,p,max}$ (°C)	$T_{c,p,min}$ (°C)	$T_{w,i}$ (°C)	Re	$\varphi_{ave,h}$ (W/kg)	$Q_{ave,h}$ (kJ/kg)
1	90 wt% SAT	3,8	22	54,3	54,3	13,6-12,8	3000	42	93
2	90 wt% SAT	3,8	27,5	55,4	51,8	12-10,3	10200	55	124
3	90 wt% SAT	3,8	40	55,9	55,9	-	-	-	-
4	90 wt% SAT	3,8	54,5	55,2	55,2	-	-	-	-
5	89 wt% SAT, 1 wt% CMC	3,6	39,5	54,5	51,1	19-9,8	5400	-	-
6	89 wt% SAT, 1 wt% CMC	3,6	51,6	52,8	50,4	22-8,3	-	-	-
7	89 wt% SAT, 1 wt% CMC	3,6	37,5	54	50	25-10	-	-	-
8	89 wt% SAT, 1 wt% CMC	3,6	34,2	53,7	50,4	-	-	-	-
9	89 wt% SAT, 1 wt% CMC	3,6	32,1	53,9	50,8	-	-	-	-
10	89 wt% SAT, 1 wt% CMC	3,6	14,3	49,9	49,5	7-6,7	19900	40	92

Experiment no.	Composition of PCM	PCM mass (kg)	T_{sc} (ºC)	$T_{c,p,max}$ (ºC)	$T_{c,p,min}$ (ºC)	$T_{w,i}$ (ºC)	Re	$\varphi_{ave,h}$ (W/kg)	$Q_{ave,h}$ (kJ/kg)
11	89 wt% SAT, 1 wt% CMC	3,6	37,3	54,3	53,6	9,9-6,7	19900	53	113
12	89 wt% SAT, 1 wt% CMC	3,6	52	52,2	-	9	8000	-	-
13	89 wt% SAT, 1 wt% CMC	3,6	16,4	50,8	50,2	10-7,3	12000	39	91
14	89 wt% SAT, 1 wt% CMC	3,6	50,9	54,8	54,1	-	-	-	-
15	89 wt% SAT, 1 wt% CMC	3,6	45,5	54,4	54,3	-	-	-	-
16	89 wt% SAT, 1 wt% CMC	3,6	15,7	48,9	48,8	9,3-8,4	6500	40	91
17	89 wt% SAT, 1 wt% CMC	3,6	23,3	51	51	12,2-7,3	12000	48	107
18	89 wt% SAT, 1 wt% CMC	3,6	51,5	52	51,5	8,2	6900	-	-
19	89 wt% SAT, 1 wt% CMC	3,6	36,1	53,4	53	22-10	4300	45	94
20	89 wt% SAT, 1 wt% CMC	3,6	9,6	46,1	46,1	7-6,3	9700	38	87
21	89 wt% SAT, 1 wt% CMC	3,6	17,9	49,6	48,9	16,4	800	29	60
22	89 wt% SAT, 1 wt% CMC	3,6	14,7	48,3	47,7	7,2-6	17000	47	106
23	89 wt% SAT, 1 wt% CMC	3,6	19,2	48,7	48,3	9,4	14400	42	96
24	89 wt% SAT, 1 wt% CMC	3,6	42,4	53,8	53,1	-	-	-	-
25	89 wt% SAT, 1 wt% CMC	3,6	23,3	50,5	50,2	23-17,6	400	25	50

Experiment no.	Composition of PCM	PCM mass (kg)	T_{sc} (ºC)	$T_{c,p,max}$ (ºC)	$T_{c,p,min}$ (ºC)	$T_{w,i}$ (ºC)	Re	$\varphi_{ave,h}$ (W/kg)	$Q_{ave,h}$ (kJ/kg)
26	89 wt% SAT, 1 wt% CMC	3,6	18,5	49,1	48,4	7,6-4,3	33000	70	160
27	89 wt% SAT, 1 wt% CMC	3,6	17	48,3	48,3	10,4-7,6	4700	41	91
28	89 wt% SAT, 1 wt% CMC	3,6	24,5	50,9	49,8	5,3	12700	52,2	118
29	89 wt% SAT, 1 wt% CMC	3,6	24,8	51,1	50,6	14,3-6,5	19000	-	-
30	89 wt% SAT, 1 wt% CMC	3,6	32	53	51,4	5	17400	60	134

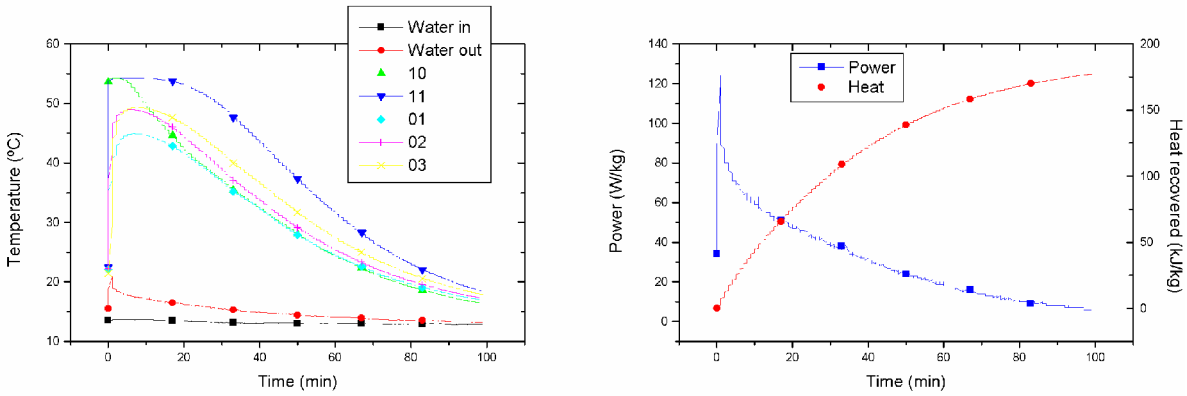

Figure A1. Experiment no. 1

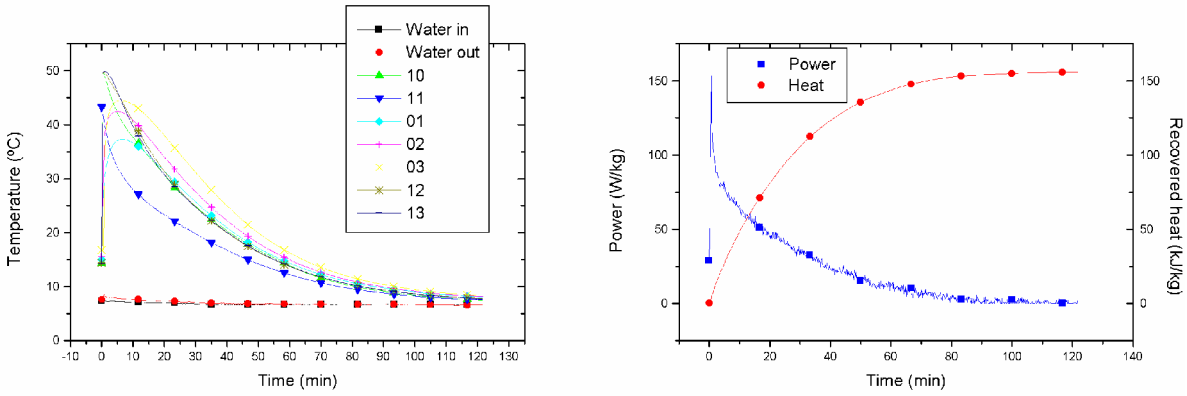

Figure A2. Experiment no. 10

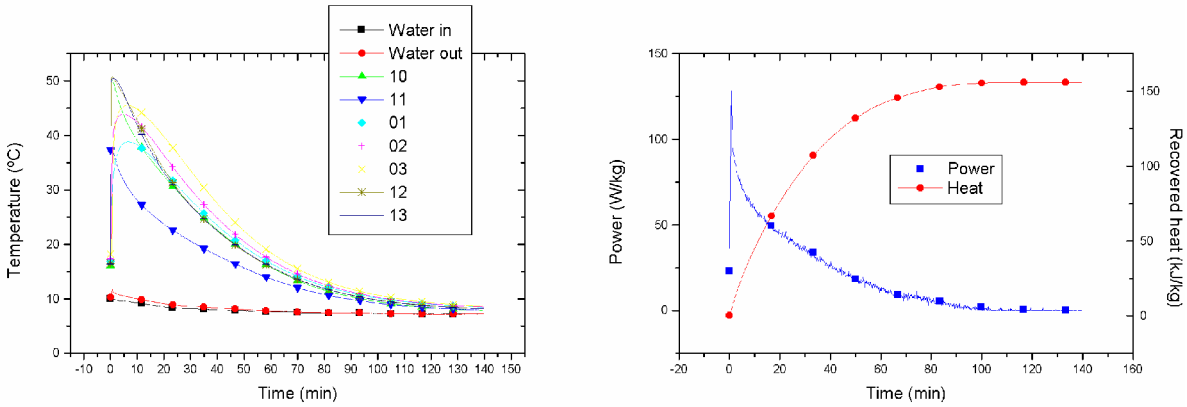

Figure A3. Experiment no. 13

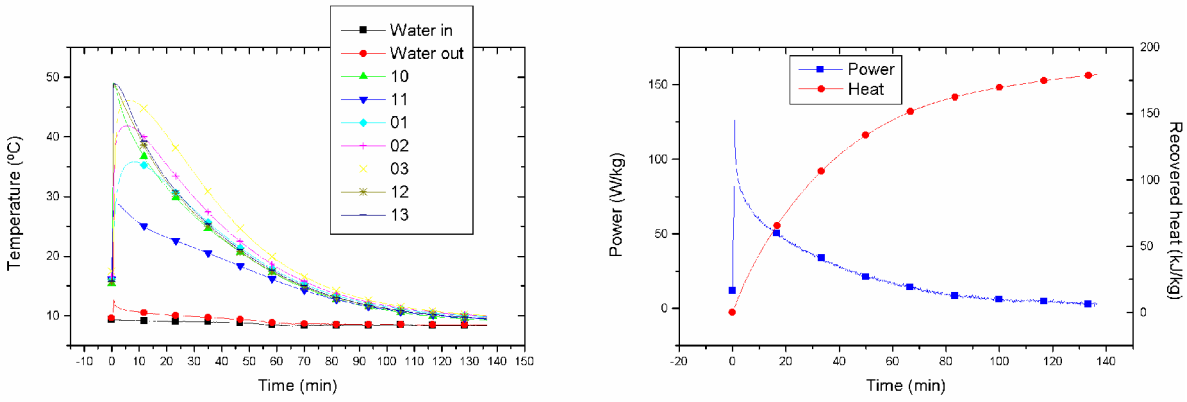

Figure A4. Experiment no. 16

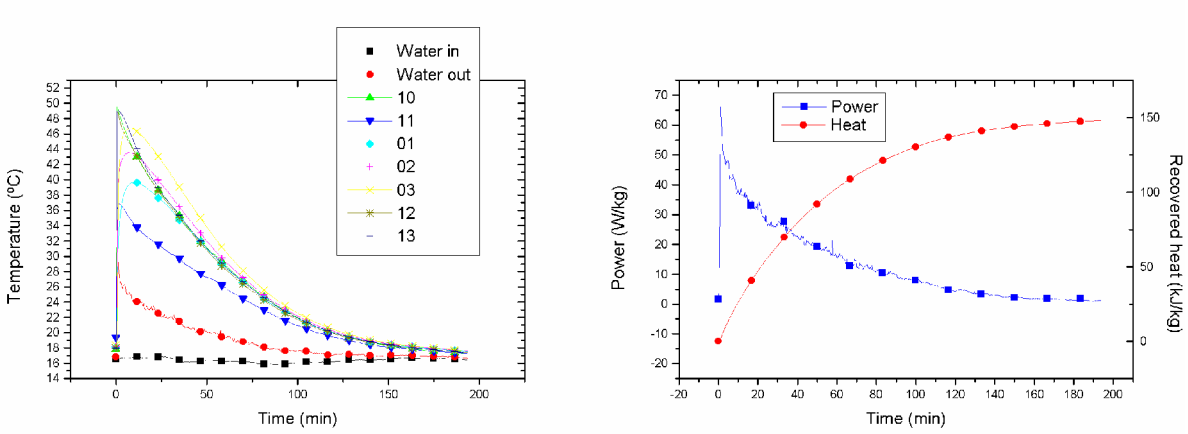

Figure A5. Experiment no. 21

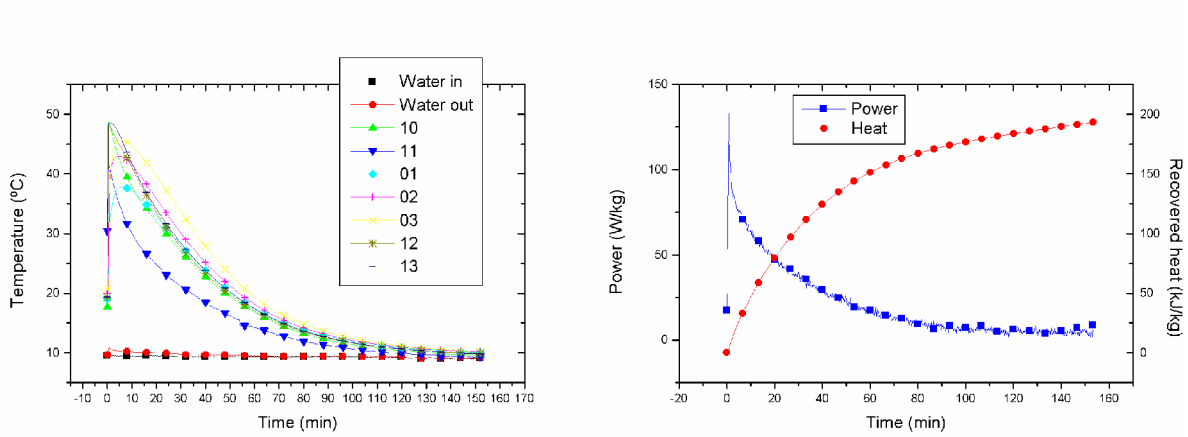

Figure A6. Experiment no. 23

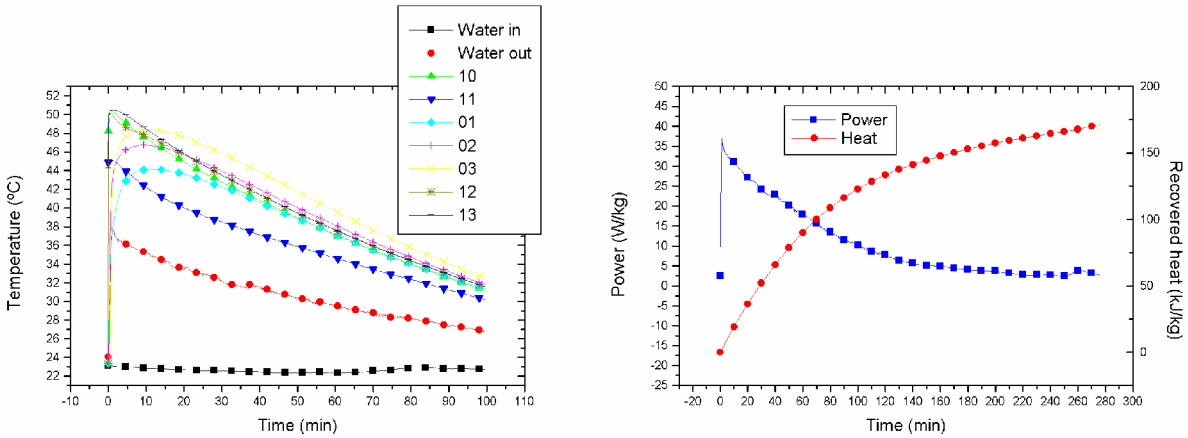

Figure A7. Experiment no. 25

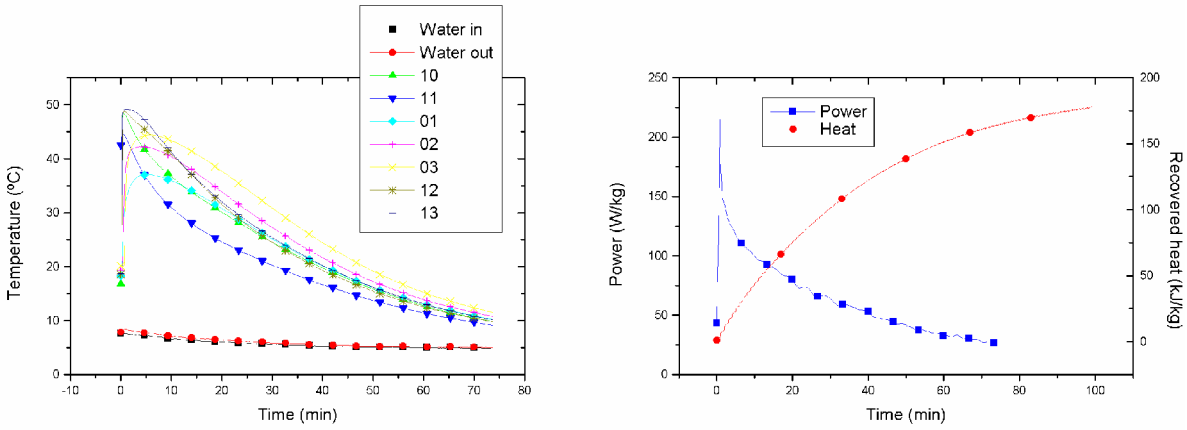

Figure A8. Experiment no. 26

APPENDIX B

Experiments with the new brush heat exchanger A yielded 11 crystallizations, but as premature crystallization occurred, commencing on sixth cycle, the data of only five experiments were recorded. Table B1 presents succesfull experiments in chronological order. The calculated $Q_{ave,h}$ is the average recovered heat within the first 60 minutes; it includes the sensible heat of supercooled SAT. Figures B1–B10 present the temperature, power and heat curves of some of the experiments. The ordinate of recovered heat in the pictures has been scaled to reduce the sensible heat; it therefore visualizes the recovered latent heat only. Bold experiment numbers refer to the intentionally crystallized experiments (in this case, all of them).

Table B1. Experimental data for brush heat exchanger A

Experiment no.	Composition of PCM	PCM mass (kg)	T_{sc} (°C)	$T_{c,p,max}$ (°C)	$T_{c,p,min}$ (°C)	$T_{w,i}$ (°C)	Re	$\varphi_{ave,h}$ (W/kg)	$Q_{ave,h}$ (kJ/kg)
51	89 wt% SAT, 1 wt% CMC	2,1	25	55	53,9	20	3500	51	137
52	89 wt% SAT, 1 wt% CMC	2,1	25	55,4	53,3	20	1500	52	136
53	89 wt% SAT, 1 wt% CMC	2,1	25	55,1	53,6	20	500	56	134
54	89 wt% SAT, 1 wt% CMC	2,1	25	55,3	53,9	20	5000	55	148
55	89 wt% SAT, 1 wt% CMC	2,1	50	56,3	55	50	3500	23	42

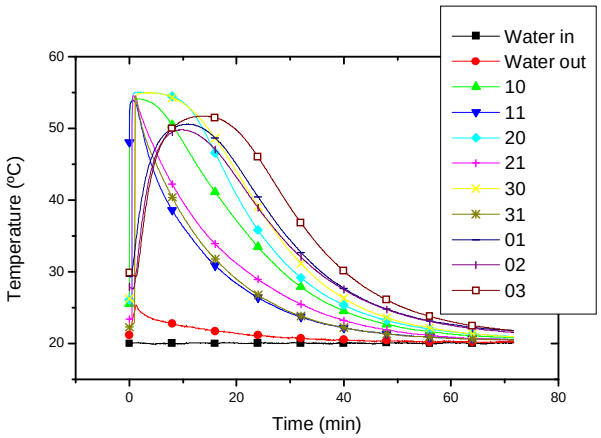

Figure B1. Temperature curves of experiment no. 51

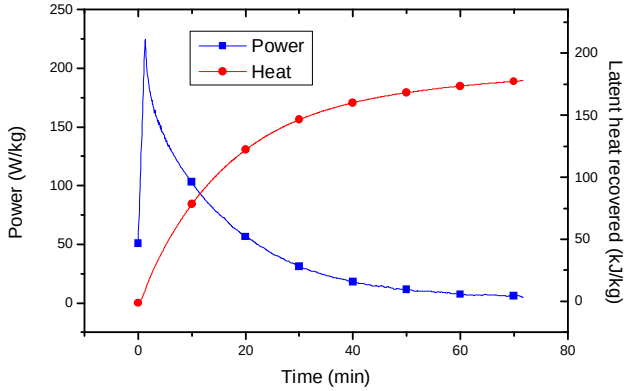

Figure B2. Power and heat curves of experiment no. 51

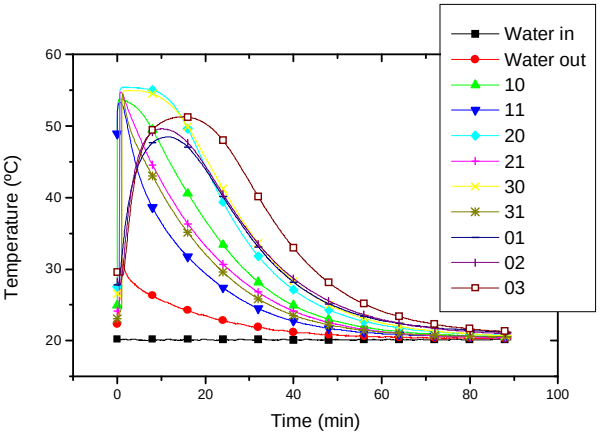

Figure B3. Temperature curves of experiment no. 52

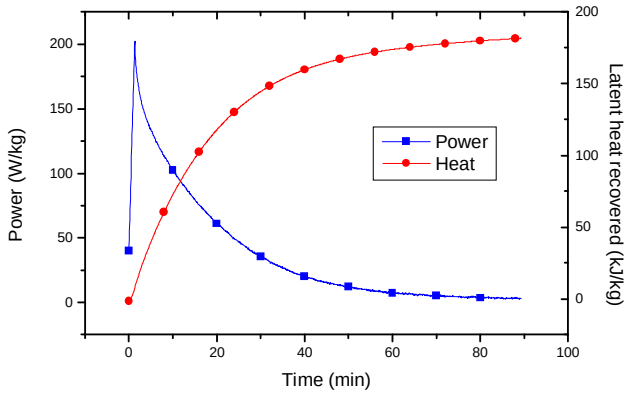

Figure B4. Power and heat curves of experiment no. 52

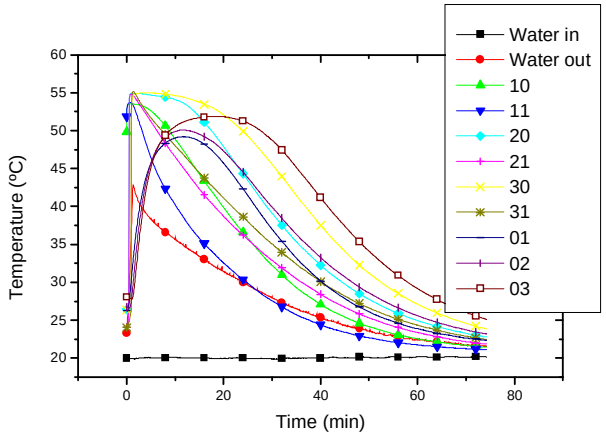

Figure B5. Temperature curves of experiment no. 53

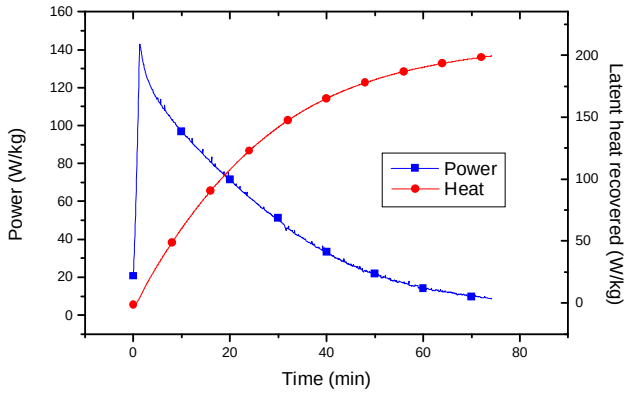

Figure B6. Power and heat curves of experiment no. 53

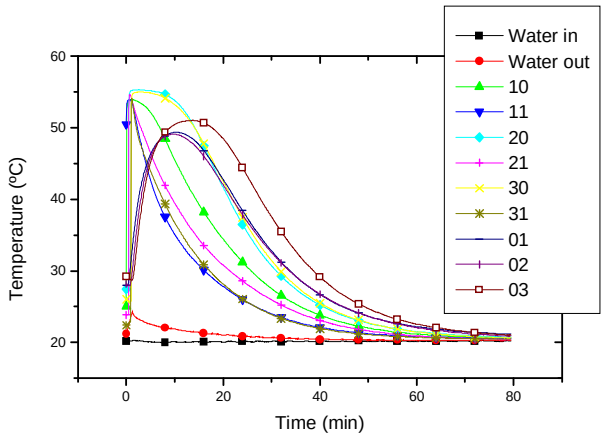

Figure B7. Temperature curves of experiment no. 54

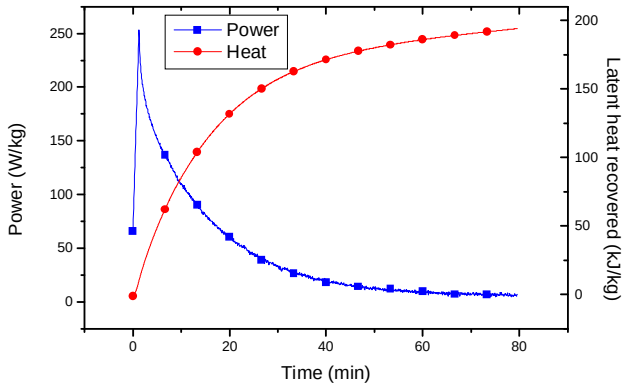

Figure B8. Power and heat curves of experiment no. 54

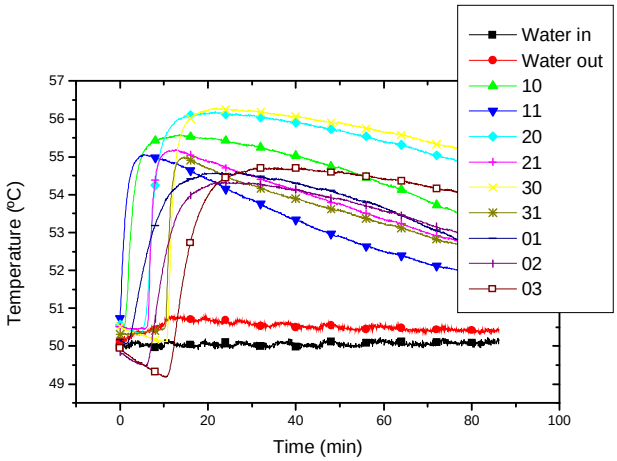

Figure B9. Temperature curves of experiment no. 55

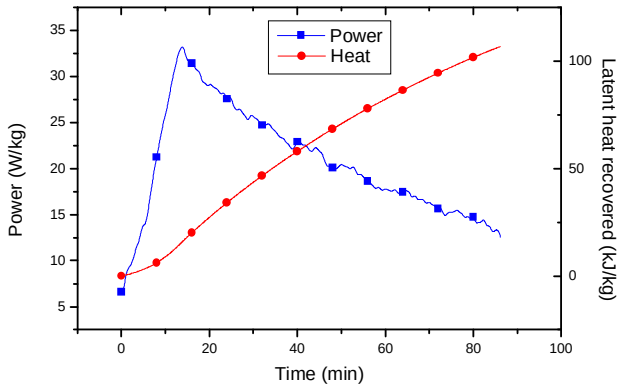

Figure B10. Power and heat curves of experiment no. 55

APPENDIX C

Measurement with brush heat exchanger B yielded a total of 24 recorded data sets. Table C1 summarizes the experimental properties. As with BHX A (Appendix B), calculated $Q_{ave,h}$ includes the sensible heat, but in the heat curves in Figures C1–C18 only the latent heat is included. Bold experiment numbers refer to the intentionally crystallized experiments.

Table C1. Experiments with brush heat exchanger B

Experiment no.	Composition of PCM	PCM mass (kg)	T_{sc} (ºC)	$T_{c,p,max}$ (ºC)	$T_{c,p,min}$ (ºC)	$T_{w,i}$ (ºC)	Re	$\varphi_{ave,h}$ (W/kg)	$Q_{ave,h}$ (kJ/kg)
63	89 wt% SAT, 1 wt% CMC	2,3	50,5	56,8	55,9	-	-	-	-
64	89 wt% SAT, 1 wt% CMC	2,3	35	56,7	54,4	20	3500	61	167
65	89 wt% SAT, 1 wt% CMC	2,3	29-52	57,1	54,6	-	-	-	-
66	89 wt% SAT, 1 wt% CMC	2,3	35	55,2	53,7	20	3500	60	163
67	89 wt% SAT, 1 wt% CMC	2,3	35	55,5	54,1	20	3500	65	172
68	89 wt% SAT, 1 wt% CMC	2,3	-	-	-	-	-	-	-
69	89 wt% SAT, 1 wt% CMC	2,3	44-32	55,3	53	20	2900	62	166
70	89 wt% SAT, 1 wt% CMC	2,3	48-52	55,7	54,4	-	-	-	-
71	89 wt% SAT, 1 wt% CMC	2,3	49-54	55,5	54	-	-	-	-
72	89 wt% SAT, 1 wt% CMC	2,3	48-54	55	53,5	-	-	-	-

Experiment no.	Composition of PCM	PCM mass (kg)	T_{sc} (ºC)	$T_{c,p,max}$ (ºC)	$T_{c,p,min}$ (ºC)	$T_{w,i}$ (ºC)	Re	$\varphi_{ave,h}$ (W/kg)	$Q_{ave,h}$ (kJ/kg)
73	89 wt% SAT, 1 wt% CMC	2,3	26	55,9	49,2	20	2900	52	141
74	89 wt% SAT, 1 wt% CMC	2,3	-	-	-	-	-	-	-
75	89 wt% SAT, 1 wt% CMC	2,3	26	56	49,3	20	5000	128	152
76	89 wt% SAT, 1 wt% CMC	2,3	25	55,4	49,3	20	1500	109	127
77	89 wt% SAT, 1 wt% CMC	2,3	26	55,6	49,8	20	500	50	120
78	89 wt% SAT, 1 wt% CMC	2,3	46	56,8	50,8	20	3500	74	193
79	89 wt% SAT, 1 wt% CMC	2,3	25	55,6	50,5	20	3500	50	138
80	89 wt% SAT, 1 wt% CMC	2,3	35	56,6	52,1	20	3500	138	163
81	89 wt% SAT, 1 wt% CMC	2,3	50	56,2	51,1	50	3500	22	41
82	89 wt% SAT, 1 wt% CMC	2,3	-	-	-	-	-	-	-
83	89 wt% SAT, 1 wt% CMC	2,3	17	54,8	46,7	5,6	3500	63	176
84	90 wt% SAT	2,4	25	56,6	48,6	*<thermocouple error>*			
85	90 wt% SAT	2,4	39-50	56,8	48,7	20	3500	69	185
86	90 wt% SAT	2,4	27	57,5	49,7	20	3500	52	142

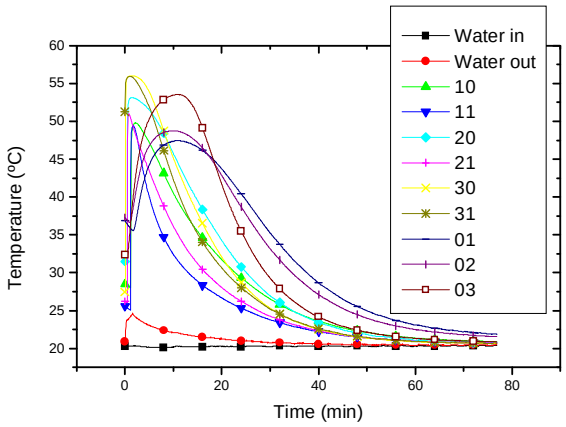

Figure C1. Temperature curves of experiment no. 75

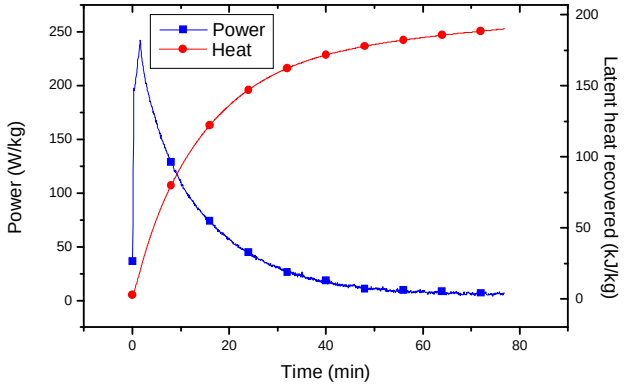

Figure C2. Power and heat curves of experiment no. 75

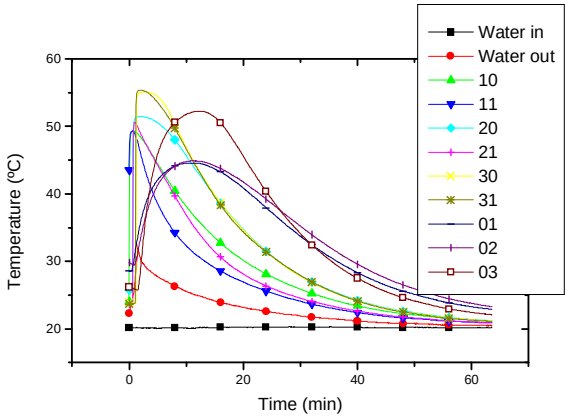

Figure C3. Temperature curves of experiment no. 76

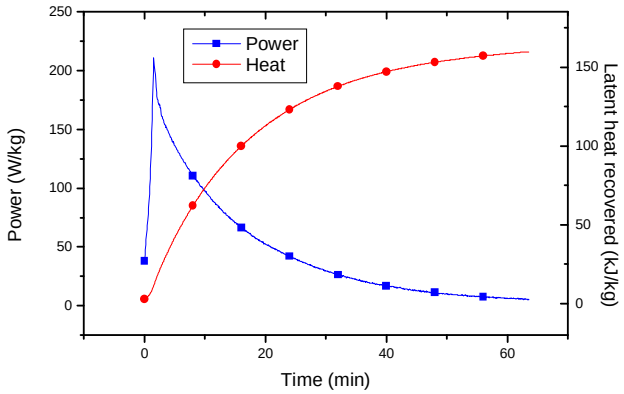

Figure C4. Power and heat curves of experiment no. 76

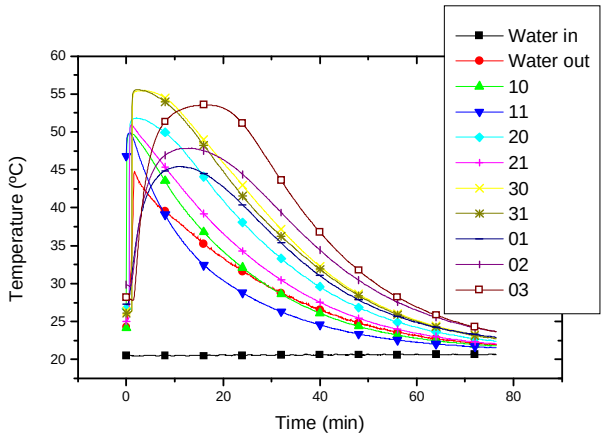

Figure C5. Temperature curves of experiment no. 77

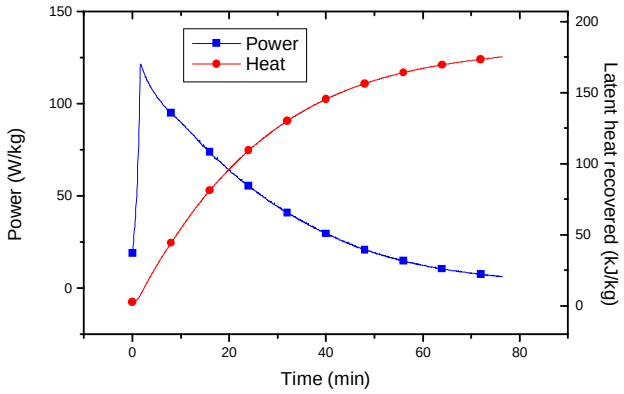

Figure C6. Power and heat curves of experiment no. 77

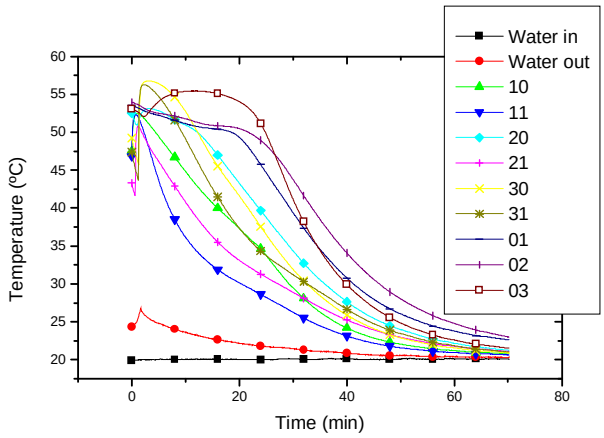

Figure C7. Temperature curves of experiment no. 78

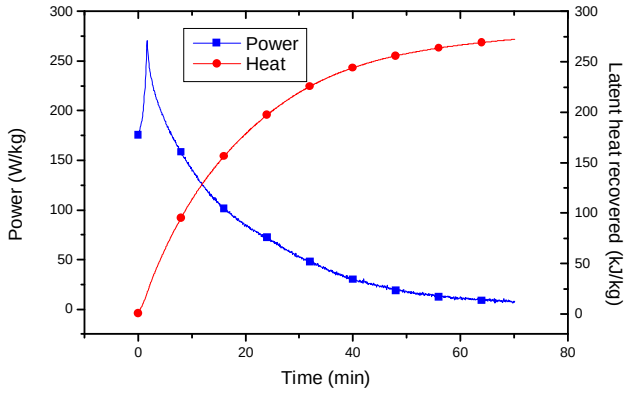

Figure C8. Power and heat curves of experiment no. 78

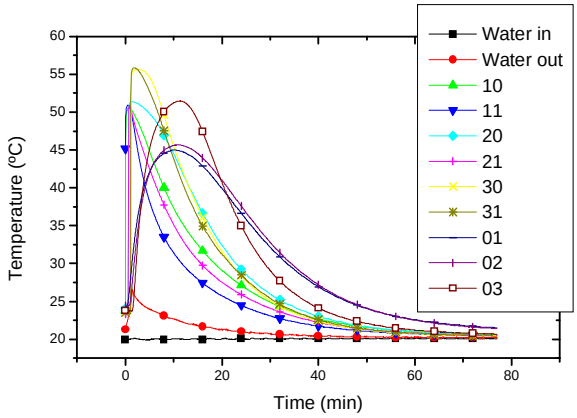

Figure C9. Temperature curves of experiment no. 79

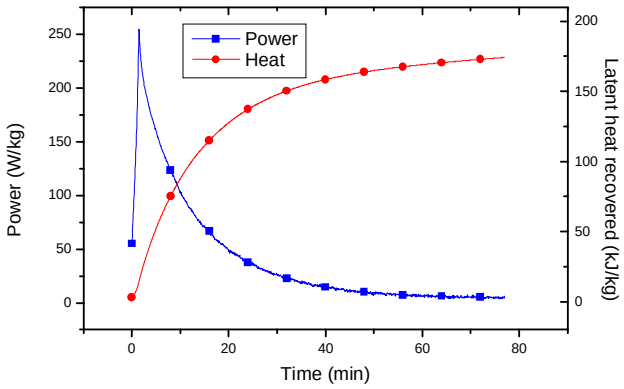

Figure C10. Power and heat curves of experiment no. 79

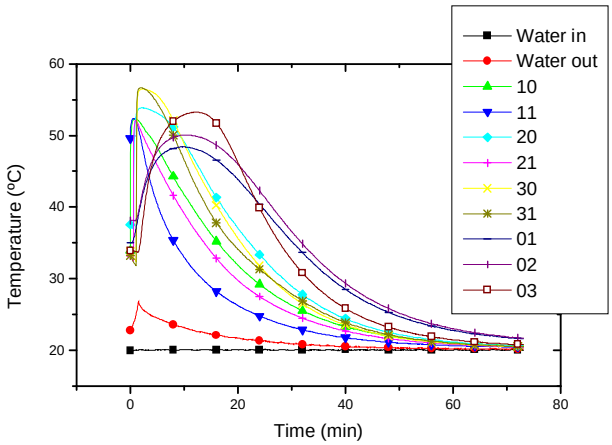

Figure C11. Temperature curves of experiment no. 80

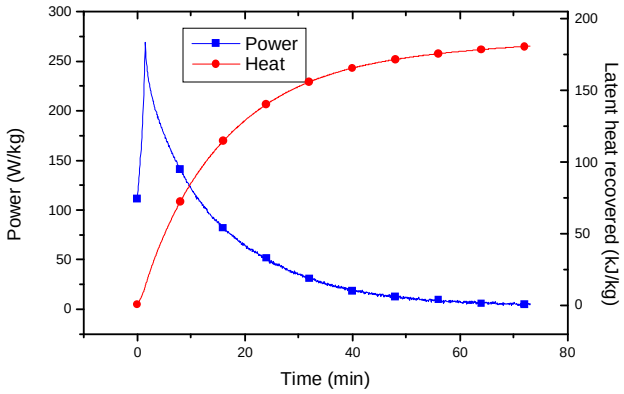

Figure C12. Power and heat curves of experiment no. 80

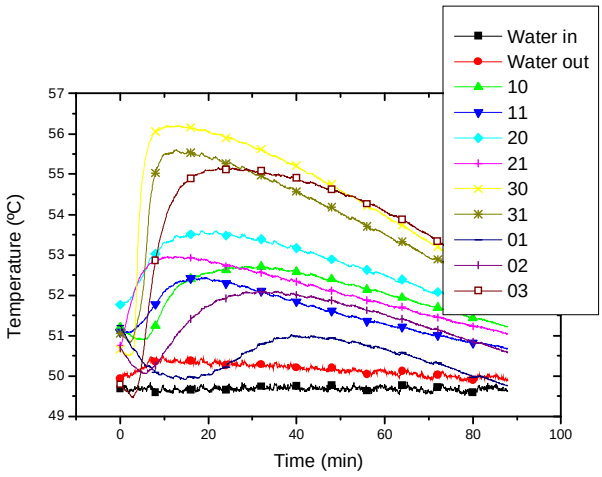

Figure C13. Temperature curves of experiment no. 81

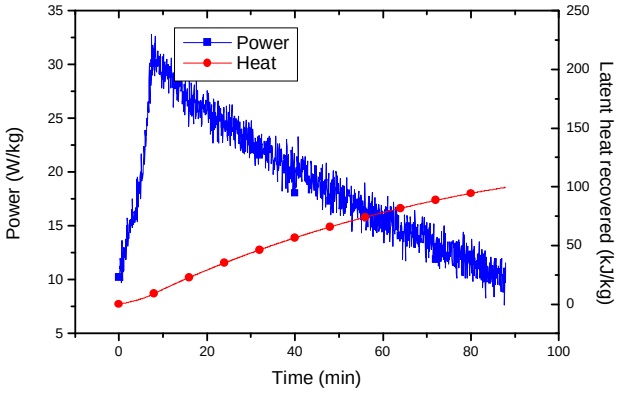

Figure C14. Power and heat curves of experiment no. 81

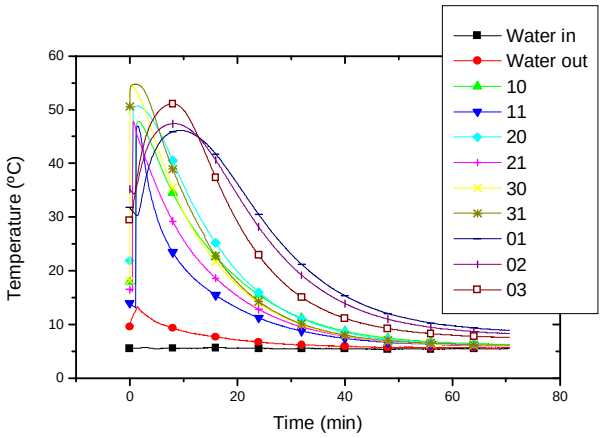

Figure C15. Temperature curves of experiment no. 83

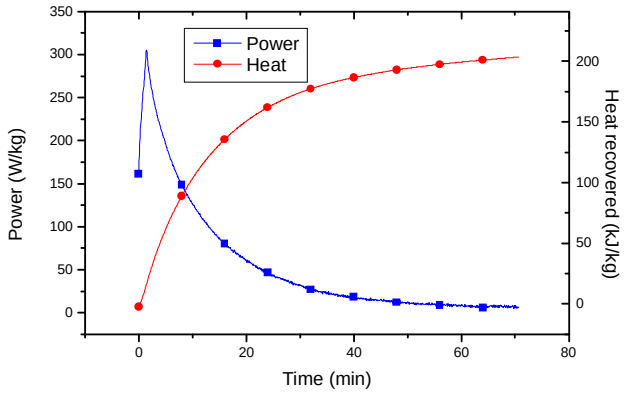

Figure C16. Power and heat curves of experiment no. 83

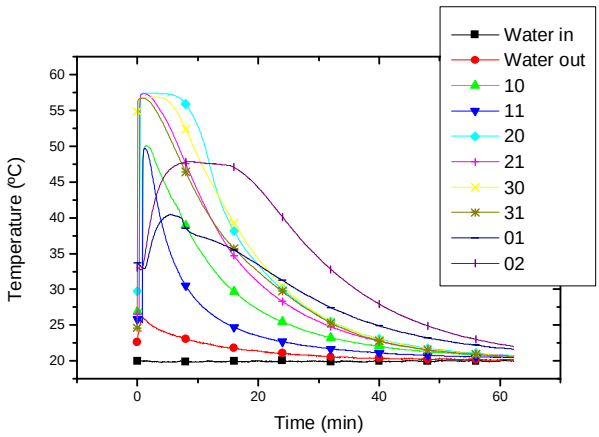

Figure C17. Temperature curves of experiment no. 86

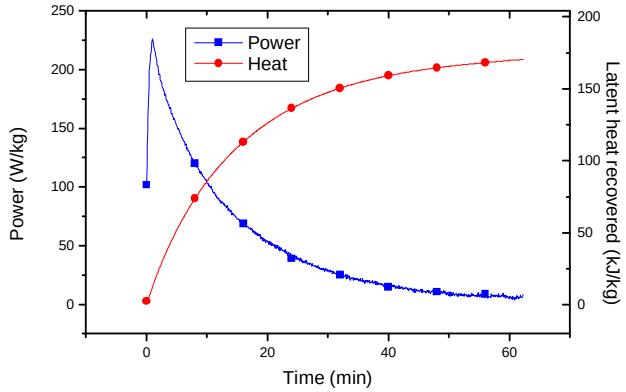

Figure C18. Power and heat curves of experiment no. 86

APPENDIX D

Total results of the experiments with the brush heat exchanger C yielding 24 data sets is presented in Table D1. Figures D1–D22 show the temperature, heat and power curves of some of the experiments. Because of the detachment of one of the surface thermocouples (thermocouple 01), this temperature is not shown in the figures. Table D1 presents the measured and calculated data of each experiment. The calculated $Q_{ave,h}$ includes the potential sensible heat, but in the figures the sensible heat is reduced only to visualize the latent heat recovered. Bold experiment numbers refer to the intentionally crystallized experiments.

Table D1. Experiments with brush heat exchanger C

Experiment no.	Composition of PCM	PCM mass (kg)	T_{sc} (ºC)	$T_{c,p,max}$ (ºC)	$T_{c,p,min}$ (ºC)	$T_{w,i}$ (ºC)	Re	$\varphi_{ave,h}$ (W/kg)	$Q_{ave,h}$ (kJ/kg)
95	89 wt% SAT, 1 wt% CMC	2,3	-	-	-	-	-	-	-
96	89 wt% SAT, 1 wt% CMC	2,3	40-49	56,7	50	-	-	-	-
97	89 wt% SAT, 1 wt% CMC	2,3	49-54	-	-	-	-	-	-
98	89 wt% SAT, 1 wt% CMC	2,3	35	56,9	52,9	20	1500	61	163
99	89 wt% SAT, 1 wt% CMC	2,3	-	-	-	-	-	-	-
100	89 wt% SAT, 1 wt% CMC	2,3	33	56,6	52,8	20	1500	61	164
101	89 wt% SAT, 1 wt% CMC	2,3	38	56,7	53,9	20	500	68	158
102	89 wt% SAT, 1 wt% CMC	2,3	25	55,7	52,4	20	3500	51	142

Experiment no.	Composition of PCM	PCM mass (kg)	T_{sc} (ºC)	$T_{c,p,max}$ (ºC)	$T_{c,p,min}$ (ºC)	$T_{w,i}$ (ºC)	Re	$\varphi_{ave,h}$ (W/kg)	$Q_{ave,h}$ (kJ/kg)
103	89 wt% SAT, 1 wt% CMC	2,3	-	-	-	-	-	-	-
104	89 wt% SAT, 1 wt% CMC	2,3	25	56,2	52	20	1500	55	148
105	89 wt% SAT, 1 wt% CMC	2,3	-	-	-	-	-	-	-
106	89 wt% SAT, 1 wt% CMC	2,3	25	56	51,8	20	500	54	129
107	89 wt% SAT, 1 wt% CMC	2,3	25	55,8	52,6	20	5000	54	153
108	89 wt% SAT, 1 wt% CMC	2,3	50	56,2	54	50	3500	26	52
109	89 wt% SAT, 1 wt% CMC	2,3	35	56,9	53,5	20	3500	67	181
110	89 wt% SAT, 1 wt% CMC	2,3	35	56,8	53,9	35	3500	48	123
111	89 wt% SAT, 1 wt% CMC	2,3	20	55,7	51,5	20	3500	49	138
112	89 wt% SAT, 1 wt% CMC	2,3	22	56,1	52,6	20	3500	51	143
113	89 wt% SAT, 1 wt% CMC	2,3	25	56,3	52,7	20	3500	52	145
114	89 wt% SAT, 1 wt% CMC	2,3	36	56,5	53,9	20	3500	63	171
115	89 wt% SAT, 1 wt% CMC	2,3	39	57,4	55,5	-	-	-	-
116	89 wt% SAT, 1 wt% CMC	2,3	25	55,8	54	20	500	54	132
117	89 wt% SAT, 1 wt% CMC	2,3	12	53,2	51,1	10	3400	49	141

Experiment no.	Composition of PCM	PCM mass (kg)	T_{sc} (ºC)	$T_{c,p,max}$ (ºC)	$T_{c,p,min}$ (ºC)	$T_{w,i}$ (ºC)	Re	$\varphi_{ave,h}$ (W/kg)	$Q_{ave,h}$ (kJ/kg)
118	89 wt% SAT, 1 wt% CMC	2,3	25	54,9	53,8	20	3500	52	146

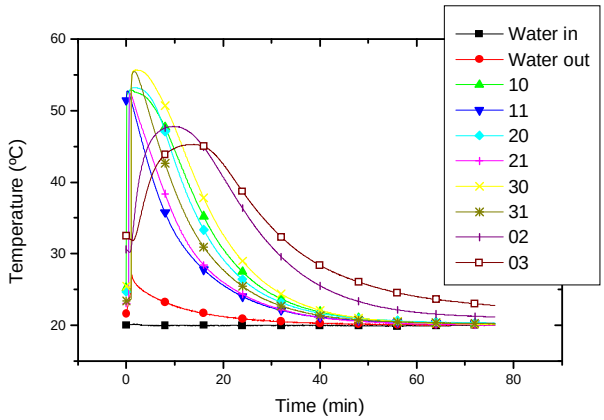

Figure D1. Temperature curves of experiment no. 102

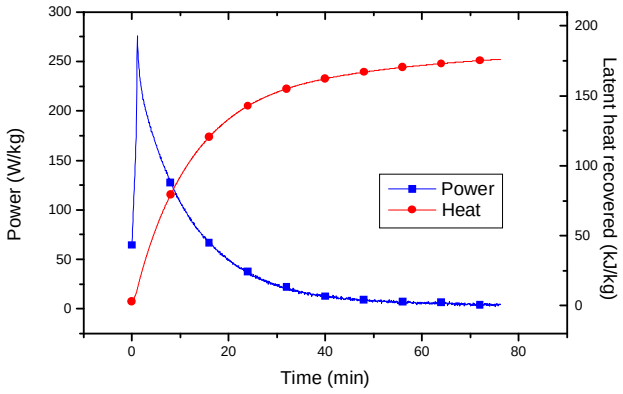

Figure D2. Power and heat curves of experiment no. 102

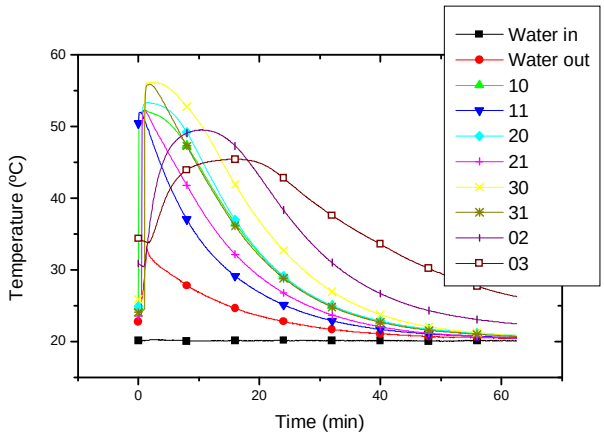

Figure D3. Temperature curves of experiment no. 104

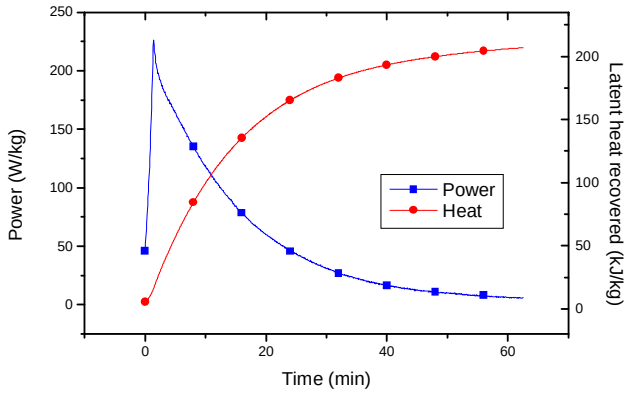

Figure D4. Power and heat curves of experiment no. 104

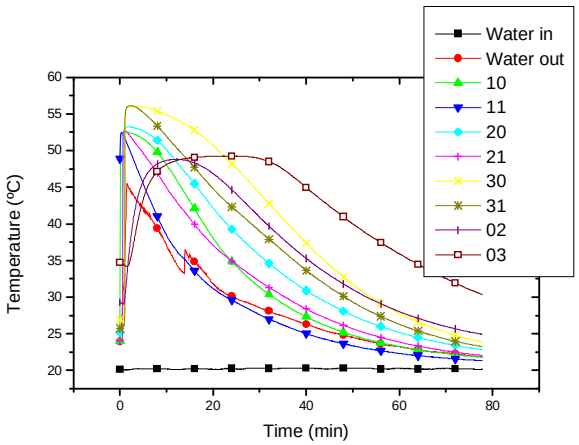

Figure D5. Temperature curves of experiment no. 107

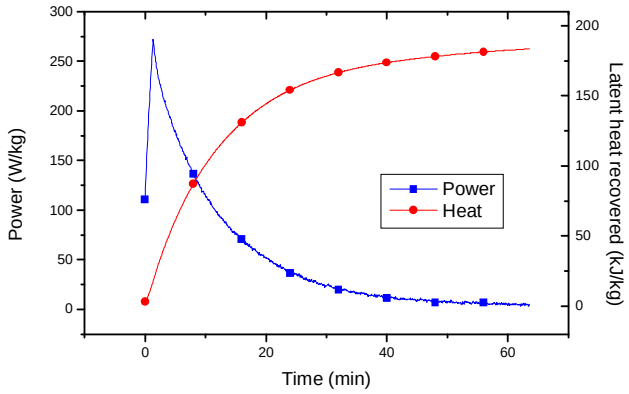

Figure D6. Power and heat curves of experiment no. 107

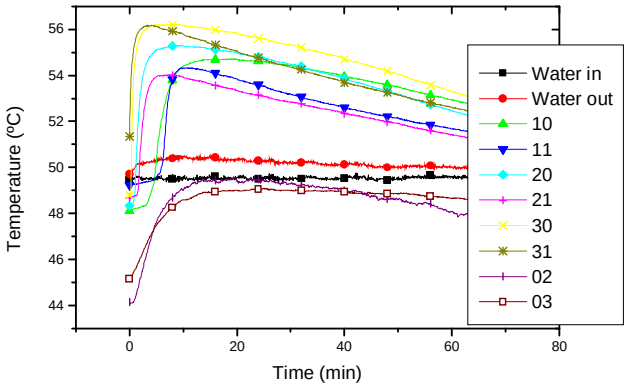

Figure D7. Temperature curves of experiment no. 108

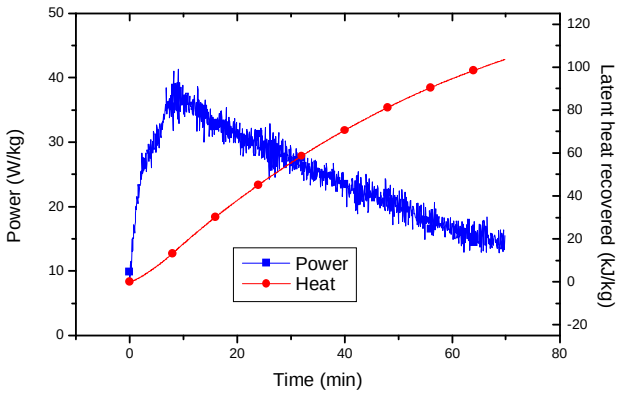

Figure D8. Power and heat curves of experiment no. 108

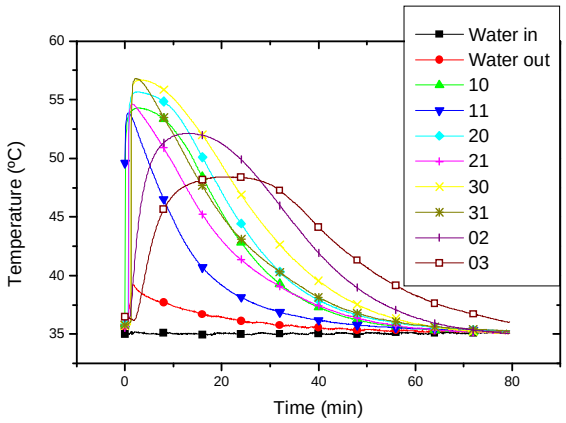

Figure D9. Temperature curves of experiment no. 110

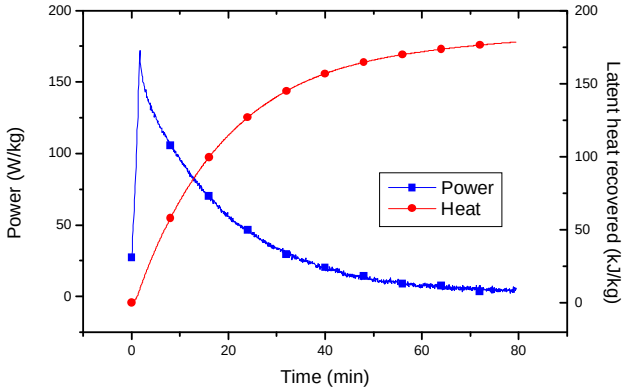

Figure D10. Power and heat curves of experiment no. 110

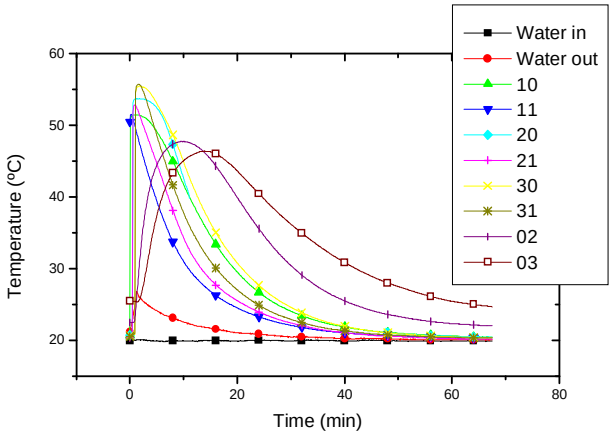

Figure D11. Temperature curves of experiment no. 111

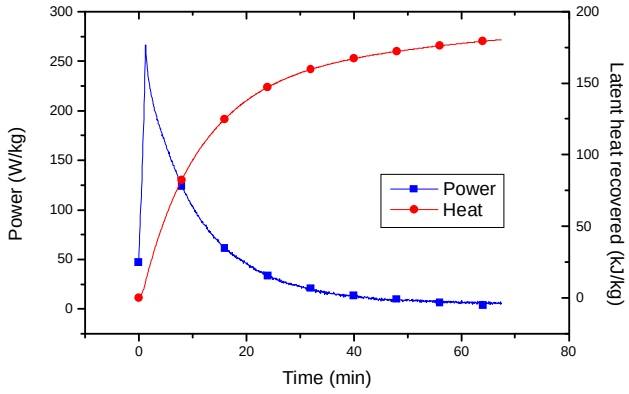

Figure D12. Power and heat curves of experiment no. 111

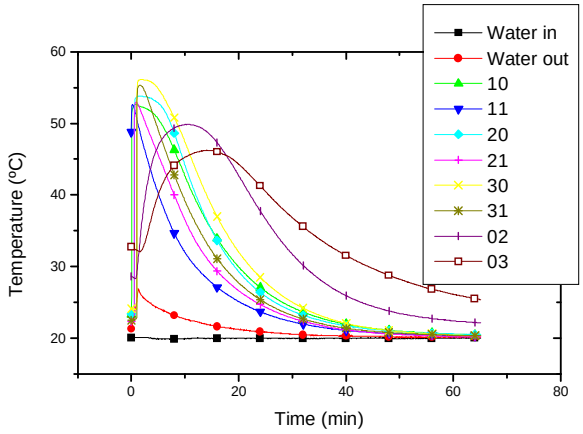

Figure D13. Temperature curves of experiment no. 112

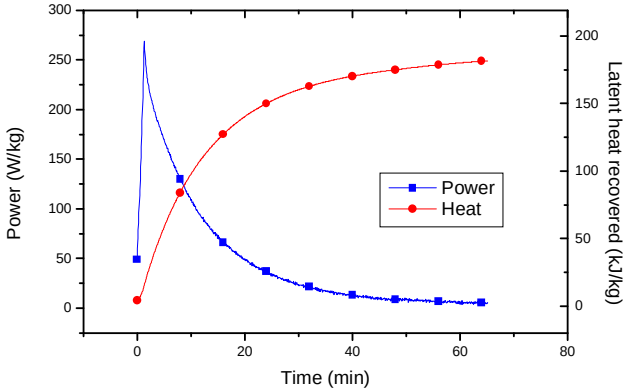

Figure D14. Power and heat curves of experiment no. 112

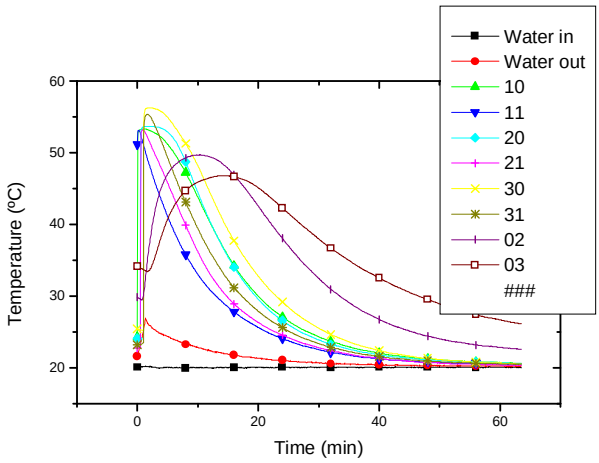

Figure D15. Temperature curves of experiment no. 113

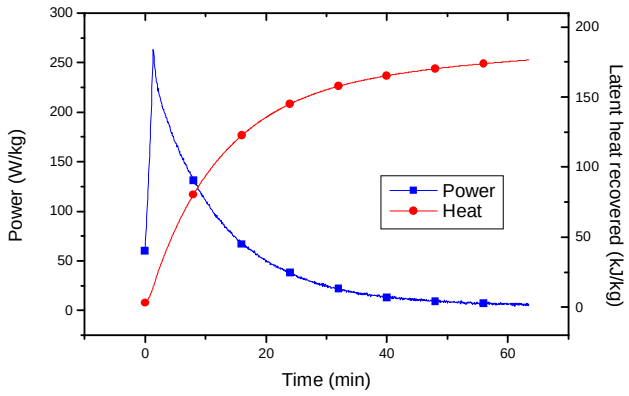

Figure D16. Power and heat curves of experiment no. 113

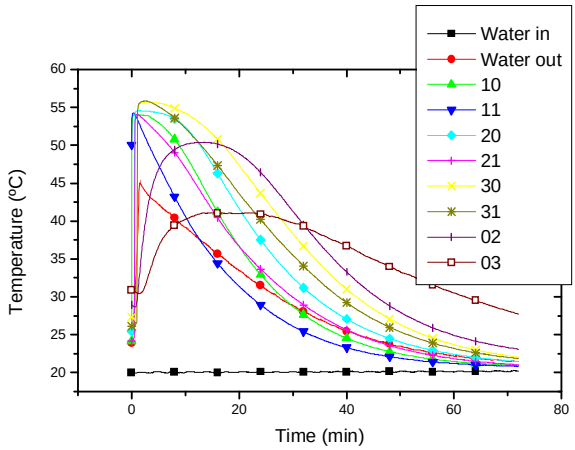

Figure D17. Temperature curves of experiment no. 116

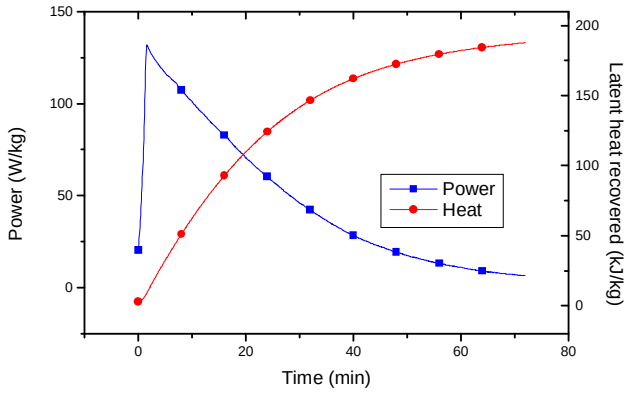

Figure D18. Power and heat curves of experiment no. 116

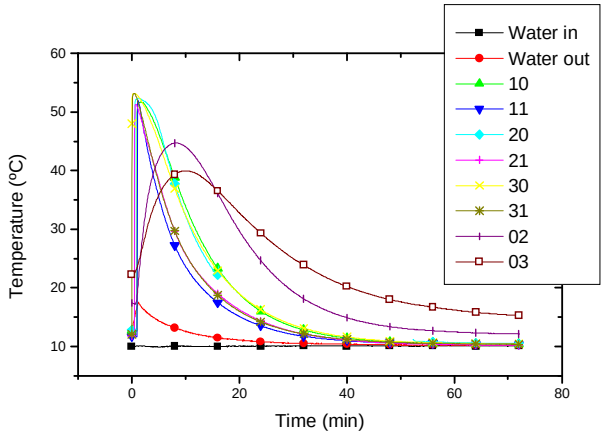

Figure D19. Temperature curves of experiment no. 117

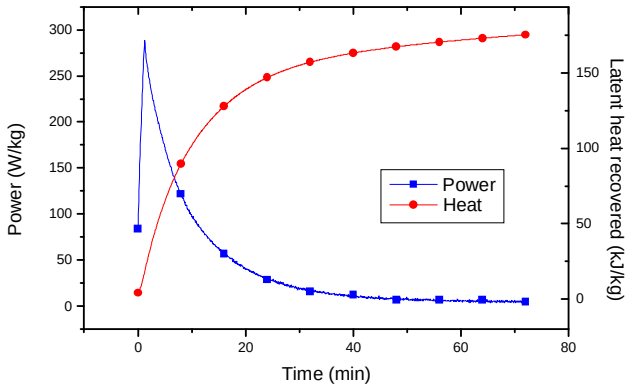

Figure D20. Power and heat curves of experiment no. 117

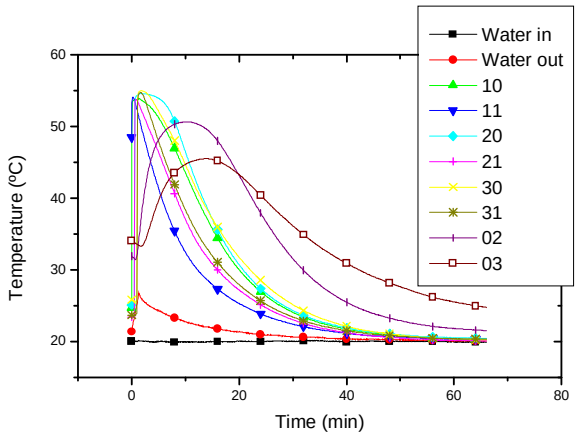

Figure D21. Temperature curves of experiment no. 118

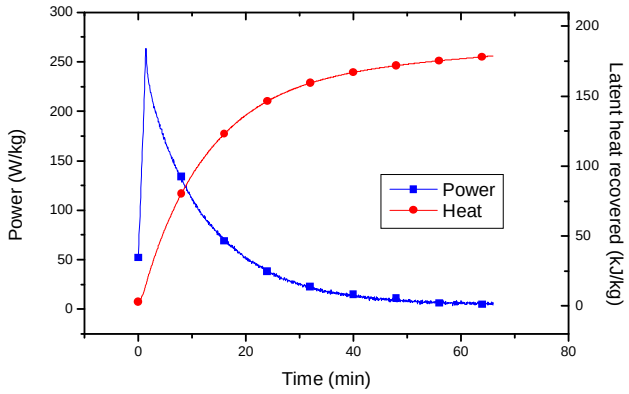

Figure D22. Power and heat curves of experiment no. 118